Geostrophic winds in Denmark: A preliminary study

Kristensen, Leif; Jensen, G.

Publication date:
1999

Document Version
Publisher's PDF, also known as Version of record

Risø–R–1145(EN)

Geostrophic Winds in Denmark: a preliminary study

Leif Kristensen and Gunnar Jensen
Risø National Laboratory

Risø National Laboratory, Roskilde, Denmark
November 1999

Abstract High-precision barometers have been deployed at six sites in Denmark, four west and two east of the Great Belt. The purpose is to establish long climatological records of the geostrophic wind as a supplement to the records of tens of years of duration of surface observations of wind, temperature, humidity etc., which have been obtained by Risø at many sites in Denmark. Three of these sites are in principle sufficient to determine an average of the magnitude and direction of the geostrophic wind inside the triangle formed by the three sites. Ten, out of twenty possible, triangles have been selected as suitable for studying the geographical variations of the geostrophic wind. A tentative conclusion from about one year of data is that statistically the geostrophic wind decrease in magnitude when going from west toward east. The data also showed that the largest mean values of the geostrophic mean wind speed are in a direction sector from 285° to 315°. The Weibull parameters were calculated for all ten triangles. The curvature of the isobars were determined by using simultaneous pressure measurements at all six sites and the geostrophic and gradient winds were calculated and compared to the geostrophic wind based on three pressure measurements in one particular triangle. Combining the geostrophic wind with the surface wind measured at Tystofte in southern Zealand, the two dimensionless constants A and B in the geostrophic drag law were determined as functions of the surface friction velocity. These data suggest that $A = 0.5$ and $B = 3.5$. The surface data at Tystofte and at Børglum in Vendsyssel in northern Jutland were used to predict the geostrophic wind by applying the geostrophic drag law with these constants and the predictions were compared to the observed geostrophic wind.

ISBN 87–550–2616–8
ISSN 0106–2840

Information Service Department · Risø · 1999

Contents

1 Introduction *5*

2 Local Geometry *5*

3 The Geostrophic Wind *10*

4 The Thermal Wind *13*

5 The Gradient Wind *15*

6 The Surface Wind *18*

7 Data and Data Analysis *19*

7.1 Geostrophic Climatology *21*

7.2 Gradient and Geostrophic Wind *26*

7.3 Review of the Geostrophic Drag Law *29*

7.4 Comparison with Surface Measurements *31*

8 Concluding Remarks *35*

Acknowledgements *37*

References *38*

A Weibull Parameters *A-1*

1 Introduction

With the purpose of obtaining a climatology for the geostrophic wind climate, six stations with precision barometers of the type Vaisala PTB 200A have been established in Denmark. At all the stations the air temperature is measured as well since it is important to determine the pressure at same reference level. All measurements are consecutive 10 minute averages.

The positions are shown in Fig. 1 and listed together with the barometer altitudes in Table 1.

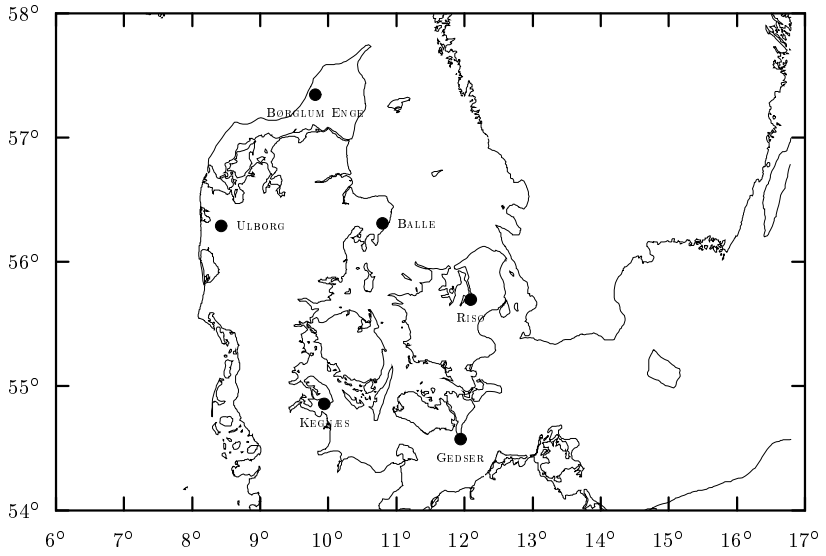

Figure 1. The six barometer positions.

The barometers have a long-term accuracy of about 0.1 HPa which at sea surface corresponds the weight per unit area of a column of air of about 0.8 m. To match this accuracy it is necessary to determine the altitudes better than about 0.5 m. Professional surveyors from LE34 in Copenhagen determined the barometer coordinates of the barometer positions to this standard.

All the six stations were in operation on April 29 1998 at 13:45.

2 Local Geometry

We want to operate in a local coordinate system where the z-axis is normal to the Earth's surface and the two horizontal axes x and y point towards East and North, respectively.

The datum ED50 corresponds to approximating the surface of the Earth with ellipsoid with the semi-axes $a = 6378.3880000$ km and $b = 6356.9119461$ km (Rasmussen 1996). This means that the eccentricity is $\epsilon = 0.0820$.

Figure 2 illustrates the situation.

Table 1. Positions and altitudes of barometers. Horizontal positions are given in the datum ED50 and the altitudes in the vertical datum DNN (Danish normal zero).

	Longitude	Latitude	Altitude (m)
Ulborg	08°25′40.9040″	56°17′27.6974″	41.49
Børglum	09°48′36.5570″	57°20′52.5701″	14.49
Kegnæs	09°56′10.6492″	54°51′20.6491″	07.45
Balle	10°47′38.5100″	56°18′30.6509″	38.47
Gedser	11°56′34.2750″	54°34′10.8587″	02.28
Risø	12°05′22.1198″	55°41′41.3339″	08.04

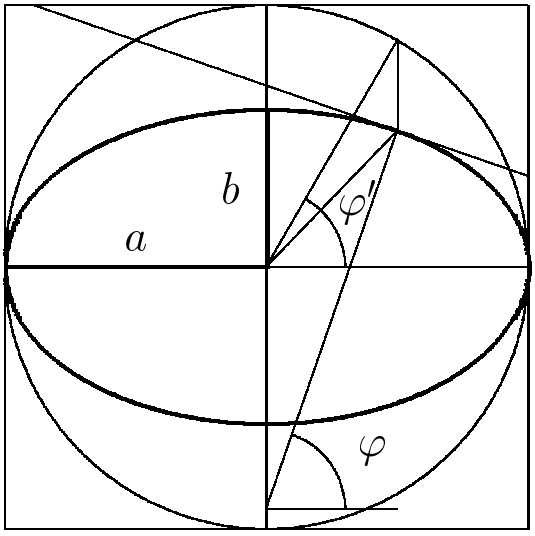

Figure 2. Sketch showing the relation between the latitude φ and the center angle φ' for an ellipse with major semi-axis a and minor semi-axis b.

The equation for the ellipse is

$$\frac{x^2}{a^2} + \frac{z^2}{b^2} = 1. \tag{1}$$

as indicated in fig. 2, a point on the ellipse can be characterized by the angle φ'. However, the latitude φ is defined as the complementary angle to the angle between the normal and the Earth's axis. We want to determine the relation between φ and φ'.

The point coordinates are

$$\left\{ \begin{array}{c} x \\ z \end{array} \right\} = \left\{ \begin{array}{c} a\cos\varphi' \\ b\sin\varphi' \end{array} \right\} \tag{2}$$

and the equation for the tangent and the normal become

$$\frac{x\cos\varphi'}{a} + \frac{z\sin\varphi'}{b} = 1 \tag{3}$$

and

$$\frac{x\sin\varphi'}{b} - \frac{z\cos\varphi'}{a} = \cos\varphi'\sin\varphi'\left\{\frac{a}{b} - \frac{b}{a}\right\}, \tag{4}$$

respectively.

Referring to Fig. 2, simple geometry leads to

$$\sin\varphi = \frac{\sin\varphi'}{\sqrt{1-\epsilon^2\cos^2\varphi'}}, \tag{5}$$

where

$$\epsilon = \sqrt{1-\frac{b^2}{a^2}} \tag{6}$$

is the eccentricity of the ellipse.

It follows that

$$\cos\varphi = \frac{\sqrt{1-\epsilon^2}\cos\varphi'}{\sqrt{1-\epsilon^2\cos^2\varphi'}}. \tag{7}$$

As a consequence of the smallness of ϵ a first-order expansion in ϵ^2 of (5) and (7) should suffice. We get

$$\cos\varphi = (1-\frac{\epsilon^2}{2}\sin^2\varphi')\ \cos\varphi' \tag{8}$$

and

$$\sin\varphi = (1+\frac{\epsilon^2}{2}\cos^2\varphi')\ \sin\varphi'. \tag{9}$$

Actually, we want φ' expressed in terms of φ and, to the same approximation, we have

$$\cos\varphi' = (1+\frac{\epsilon^2}{2}\sin^2\varphi)\ \cos\varphi \tag{10}$$

and

$$\sin\varphi' = (1-\frac{\epsilon^2}{2}\cos^2\varphi)\ \sin\varphi \tag{11}$$

Considering the Earth as a compressed, axisymmetric ellipsoid, we can specify a position on the surface in the geocentric coordinate system ($\boldsymbol{i}_0$, $\boldsymbol{j}_0$, $\boldsymbol{k}_0$) by

$$\boldsymbol{r} = a\cos\varphi'\cos\lambda\,\boldsymbol{i}_0 + a\cos\varphi'\sin\lambda\,\boldsymbol{j}_0 + b\sin\varphi'\,\boldsymbol{k}_0, \tag{12}$$

where λ is the longitude.

Using a as the length unit and applying the approximation

$$\frac{b}{a} = \sqrt{1-\epsilon^2} = 1 - \frac{\epsilon^2}{2}, \tag{13}$$

we may express $\boldsymbol{r}$ in terms of the latitude and the eccentricity as

$$\begin{aligned} \boldsymbol{r} &= (1 + \frac{\epsilon^2}{2}\sin^2\varphi)\cos\varphi\cos\lambda\,\boldsymbol{i}_0 + (1 + \frac{\epsilon^2}{2}\sin^2\varphi)\cos\varphi\sin\lambda\,\boldsymbol{j}_0 \\ &\quad + (1 - \frac{\epsilon^2}{2}[1+\cos^2\varphi])\sin\varphi\,\boldsymbol{k}_0. \end{aligned} \tag{14}$$

A differential distance δs can now be expressed in terms of differential increments $\delta\varphi$ and $\delta\lambda$ in latitude φ and longitude λ:

$$\delta s^2 \equiv \delta\,\boldsymbol{r}\cdot\delta\,\boldsymbol{r} = \{1-\epsilon^2(2-3\sin^2\varphi)\}\,\delta\varphi^2 + \{1+\epsilon^2\sin^2\varphi\}\cos^2\varphi\,\delta\lambda^2. \tag{15}$$

To define the local coordinate system at (φ,λ), we must determine the length of the vector $\boldsymbol{r}$.

We find

$$|\,\boldsymbol{r}|^2 = 1 - \epsilon^2\sin^2\varphi. \tag{16}$$

The vertical unit vector $\boldsymbol{k}$ thus becomes

$$\begin{aligned} \boldsymbol{k} &= \left\{1+\epsilon^2\sin^2\varphi\right\}\cos\varphi\cos\lambda\,\boldsymbol{i}_0 + \left\{1+\epsilon^2\sin^2\varphi\right\}\cos\varphi\sin\lambda\,\boldsymbol{j}_0 \\ &\quad + \left\{1-\epsilon^2\cos^2\varphi\right\}\sin\varphi\,\boldsymbol{k}_0. \end{aligned} \tag{17}$$

In the tangent plane the unit vector $\boldsymbol{i}$ pointing East is

$$\boldsymbol{i} = -\sin\lambda\,\boldsymbol{i}_0 + \cos\lambda\,\boldsymbol{j}_0. \tag{18}$$

Finally, the unit vector pointing North in the tangent plane can be determined as

$$\begin{aligned} \boldsymbol{j} &= \boldsymbol{k}\times\boldsymbol{i} \\ &= -\left\{1-\epsilon^2\cos^2\varphi\right\}\sin\varphi\cos\lambda\,\boldsymbol{i}_0 - \left\{1-\epsilon^2\cos^2\varphi\right\}\sin\varphi\sin\lambda\,\boldsymbol{j}_0 \\ &\quad + \left\{1+\epsilon^2\sin^2\varphi\right\}\cos\varphi\,\boldsymbol{k}_0. \end{aligned} \tag{19}$$

We now define a the local reference coordinate systems in terms of the latitude φ_M and the longitude λ_M. The geocentric coordinate system is defined by the unit vectors $\boldsymbol{i}_0$, $\boldsymbol{j}_0$, and $\boldsymbol{k}_0$. The local reference system is then given by (18), (19) and (**??**) with φ and λ replaced by φ_M and λ_M:

$$\boldsymbol{i} = -\sin\lambda_M\,\boldsymbol{i}_0 + \cos\lambda_M\,\boldsymbol{j}_0, \tag{20}$$

$$\begin{aligned}\boldsymbol{j} = & -\left\{1-\epsilon^2\cos^2\varphi_M\right\}\sin\varphi_M\cos\lambda_M\,\boldsymbol{i}_0\\ & -\left\{1-\epsilon^2\cos^2\varphi_M\right\}\sin\varphi_M\sin\lambda_M\,\boldsymbol{j}_0\\ & +\left\{1+\epsilon^2\sin^2\varphi_M\right\}\cos\varphi_M\,\boldsymbol{k}_0,\end{aligned} \tag{21}$$

and

$$\begin{aligned}\boldsymbol{k} = & \left\{1+\epsilon^2\cos^2\varphi_M\right\}\cos\varphi_M\cos\lambda_M\,\boldsymbol{i}_0\\ & +\left\{1+\epsilon^2\cos^2\varphi_M\right\}\cos\varphi_M\sin\lambda_M\,\boldsymbol{j}_0\\ & +\left\{1-\epsilon^2\sin^2\varphi_M\right\}\sin\varphi_M\,\boldsymbol{k}_0.\end{aligned} \tag{22}$$

The origin of the local reference coordinate system is

$$\begin{aligned}\boldsymbol{r}_M = & \left(1+\frac{\epsilon^2}{2}\sin^2\varphi_M\right)\cos\varphi_M\cos\lambda_M\,\boldsymbol{i}_0\\ & +\left(1+\frac{\epsilon^2}{2}\sin^2\varphi_M\right)\cos\varphi_M\sin\lambda_M\,\boldsymbol{j}_0\\ & +\left(1-\frac{\epsilon^2}{2}[1+\cos^2\varphi_M]\right)\sin\varphi_M\,\boldsymbol{k}_0.\end{aligned} \tag{23}$$

We find

$$\boldsymbol{r}_M\cdot\boldsymbol{i}=0 \tag{24}$$

and

$$\boldsymbol{r}_M\cdot\boldsymbol{j}=O\left(\epsilon^4\right) \tag{25}$$

so we will ignore that $\boldsymbol{r}_M$ is not quite perpendicular to the horizontal plane at the origin of the local coordinate system.

A position (14) given by latitude φ and longitude λ can now be expressed in Cartesian coordinates in the local reference coordinate system. We find

$$x=(\boldsymbol{r}-\boldsymbol{r}_M)\cdot\boldsymbol{i}=\boldsymbol{r}\cdot\boldsymbol{i}=\left(1+\frac{\epsilon^2}{2}\sin^2\varphi\right)\cos\varphi\sin(\lambda-\lambda_M) \tag{26}$$

and

$$\begin{aligned}&y=(\boldsymbol{r}-\boldsymbol{r}_M)\cdot\boldsymbol{j}=\boldsymbol{r}\cdot\boldsymbol{j}=\\ &\left(1-\frac{\epsilon^2}{2}\left\{2\cos^2\varphi_M-\sin^2\varphi\right\}\right)\left(\cos\varphi_M\sin\varphi-\sin\varphi_M\cos\varphi\cos(\lambda-\lambda_M)\right).\end{aligned} \tag{27}$$

Sometimes we will need to determine the latitude φ_M from the components of the unit vector $\boldsymbol{k}$ given by (22).

Rewriting (22) as follows

$$\boldsymbol{k} = Z_0\,\boldsymbol{i}_0 + Z_1\,\boldsymbol{j}_0 + Z_2\,\boldsymbol{k}_0, \tag{28}$$

where

$$\left\{\begin{array}{c} Z_0 \\ Z_1 \\ Z_2 \end{array}\right\} = \left\{\begin{array}{l} \left(1+\epsilon^2\sin^2\varphi_M\right)\cos\varphi_M\cos\lambda_M \\ \left(1+\epsilon^2\sin^2\varphi_M\right)\cos\varphi_M\sin\lambda_M \\ \left(1-\epsilon^2\cos^2\varphi_M\right)\sin\varphi_M \end{array}\right\}, \tag{29}$$

we define

$$Z_c = Z_0^2 + Z_1^2 - Z_2^2 = \cos(2\varphi_M) + \epsilon^2\sin^2(2\varphi_M) + O(\epsilon^4) \tag{30}$$

$$Z_s = 2Z_2\sqrt{Z_0^2+Z_1^2} = \sin(2\varphi_M) - \epsilon^2\cos(2\varphi_M)\sin(2\varphi_M) + O(\epsilon^4). \tag{31}$$

Excluding terms of higher order in ϵ than 4, we get

$$\cos(2\varphi_M) = Z_c - \epsilon^2 Z_s^2 \tag{32}$$

and

$$\sin(2\varphi_M) = Z_s + \epsilon^2 Z_c Z_s. \tag{33}$$

3 The Geostrophic Wind

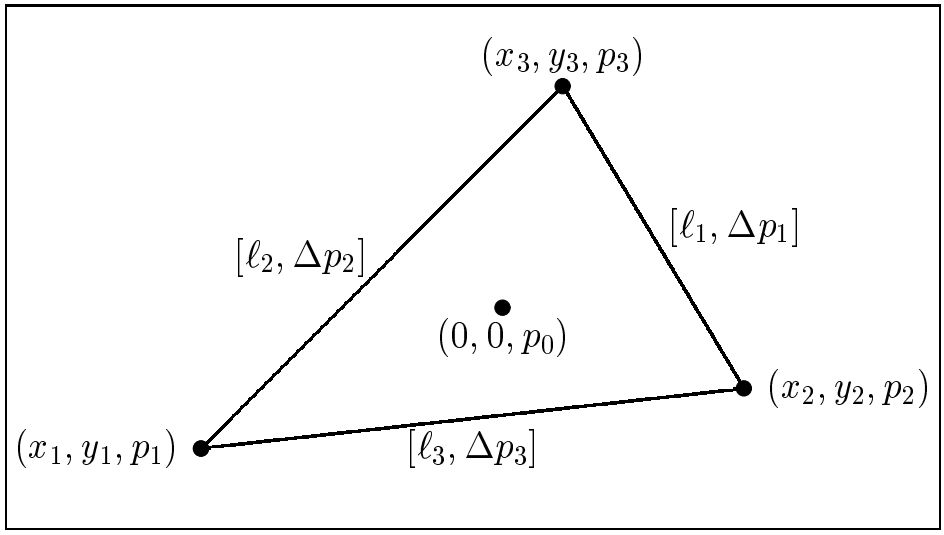

Figure 3. Triangle for determination of the geostrophic wind velocity.

The geostrophic wind velocity is given by (see e.g., Dutton (1986))

$$\boldsymbol{G} = \frac{1}{\rho f}\,\boldsymbol{k} \times \boldsymbol{\nabla}_2 p, \tag{34}$$

where

$$\boldsymbol{\nabla}_2 \equiv \boldsymbol{i}\frac{\partial}{\partial x} + \boldsymbol{j}\frac{\partial}{\partial y} \tag{35}$$

is the horizontal gradient, ρ and p are the density of air and the pressure, both at the ground, and

$$f = \Omega \sin(\varphi_M) = 1.458\ 10^{-4}\,\mathrm{s}^{-1}\ \sin(\varphi_M) \tag{36}$$

is the Coriolis parameter.

We assume that we can determine $\boldsymbol{G}$ by means of the pressure measured at three different places

$$\boldsymbol{r}_i - \boldsymbol{r}_M = x_i\,\boldsymbol{i} + y_i\,\boldsymbol{j}, \quad i = 1, 2, 3 \tag{37}$$

which are not on the same straight line in the tangent plane defined by $\boldsymbol{i}$ and $\boldsymbol{j}$. This means that, inside the triangle determined by the three points, the pressure varies linearly with the position coordinates. In other words,

$$p(x, y) = p_0 + \frac{\partial p}{\partial x}x + \frac{\partial p}{\partial y}y = p_0 + p'_x x + p'_y y. \tag{38}$$

As (34) shows, we must find the magnitude and the direction of

$$\boldsymbol{\nabla}_2 p = p'_x\,\boldsymbol{i} + p'_y\,\boldsymbol{j} \tag{39}$$

and we have the three equations

$$\left\{ \begin{array}{ccc} 1 & x_1 & y_1 \\ 1 & x_2 & y_2 \\ 1 & x_3 & y_3 \end{array} \right\} \times \left\{ \begin{array}{c} p_0 \\ p'_x \\ p'_y \end{array} \right\} = \left\{ \begin{array}{c} p_1 \\ p_2 \\ p_3 \end{array} \right\} \tag{40}$$

with the three unknowns p_0, p'_x and p'_y.

We find

$$p'_x = \frac{1}{D}\left\{p_1(y_2 - y_3) + p_2(y_3 - y_1) + p_3(y_1 - y_2)\right\} \tag{41}$$

and

$$p'_y = \frac{1}{D}\left\{p_1(x_3 - x_2) + p_2(x_1 - x_3) + p_3(x_2 - x_1)\right\}, \tag{42}$$

where D is the determinant:

$$D = \left| \begin{array}{ccc} 1 & x_1 & y_1 \\ 1 & x_2 & y_2 \\ 1 & x_3 & y_3 \end{array} \right|. \tag{43}$$

We see immediately that the direction of the geostrophic wind is given by

$$\begin{aligned}\boldsymbol{k} \times \left\{p'_x\,\boldsymbol{i} + p'_y\,\boldsymbol{j}\right\} &= -p'_y\,\boldsymbol{i} + p'_x\,\boldsymbol{j} = \\ &\frac{1}{D}\left[\{p_1(x_2-x_3)+p_2(x_3-x_1)+p_3(x_1-x_2)\}\;\boldsymbol{i}\right. \\ &\left.+\;\{p_1(y_2-y_3)+p_2(y_3-y_1)+p_3(y_1-y_2)\}\;\boldsymbol{j}\right]. \end{aligned} \tag{44}$$

The direction of the geostrophic wind vector is then

$$\begin{aligned}\alpha_G \;\;=\;\; &\arctan2(p_1(x_2-x_3)+p_2(x_3-x_1)+p_3(x_1-x_2), \\ &\qquad p_1(y_2-y_3)+p_2(y_3-y_1)+p_3(y_1-y_2)\big). \end{aligned} \tag{45}$$

The magnitude of $\boldsymbol{\nabla}_2 p$ can be expressed in terms of the lengths of the sides in the triangle

$$\begin{aligned}\ell_1 &= \sqrt{(x_3-x_2)^2+(y_3-y_2)^2} \\ \ell_2 &= \sqrt{(x_1-x_3)^2+(y_1-y_3)^2} \\ \ell_3 &= \sqrt{(x_2-x_1)^2+(y_2-y_1)^2}\end{aligned} \tag{46}$$

and the three pressures.

$$\begin{aligned}(\boldsymbol{\nabla}_2 p)^2 \;\;=\;\; &\frac{1}{4A^2}\left[\left(\ell_1^2\{p_1^2+p_2p_3\}+\ell_2^2\{p_2^2+p_3p_1\}+\ell_3^2\{p_3^2+p_1p_2\}\right)\right. \\ &\left.-\;\left(p_2p_3\{\ell_2^2+\ell_3^2\}+p_3p_1\{\ell_3^2+\ell_1^2\}+p_1p_2\{\ell_1^2+\ell_2^2\}\right)\right], \end{aligned} \tag{47}$$

where

$$A = \frac{1}{4}\sqrt{\{+\ell_1+\ell_2+\ell_3\}\{+\ell_1+\ell_2-\ell_3\}\{+\ell_1-\ell_2+\ell_3\}\{-\ell_1+\ell_2+\ell_3\}}, \tag{48}$$

according to Heron's formula, is the area of a plane triangle with the side-lengths ℓ_1, ℓ_2 and ℓ_3.

It is possible to estimate how the random errors $\delta[p_i]$ on the measurements propagate to $\boldsymbol{\nabla}_2 p$. Assuming that the measuring errors on the pressures are the same and equal to $\delta[p]$, we may use the equation

$$\delta^2[(\boldsymbol{\nabla}_2 p)^2] = \delta^2[p]\sum_{i=1}^{3}\left\{\frac{\partial}{\partial p_i}(\boldsymbol{\nabla}_2 p)^2\right\}^2. \tag{49}$$

We have

$$\frac{\partial}{\partial p_1}(\boldsymbol{\nabla}_2 p)^2 = \frac{1}{4A^2}\left\{2\ell_1^2 p_1 + (\ell_2^2-\ell_3^2-\ell_1^2)p_3 + (\ell_3^2-\ell_1^2-\ell_2^2)p_2\right\}. \tag{50}$$

Also, we have the identity

$$0 = \frac{1}{4A^2}\left\{2\ell_1^2 p_1 + (\ell_2^2 - \ell_3^2 - \ell_1^2)p_1 + (\ell_3^2 - \ell_1^2 - \ell_2^2)p_1\right\} \tag{51}$$

so that

$$\frac{\partial}{\partial p_1}(\boldsymbol{\nabla}_2 p)^2 = \frac{1}{4A^2}\left\{(\ell_2^2 - \ell_3^2 - \ell_1^2)(p_3 - p_1) + (\ell_3^2 - \ell_1^2 - \ell_2^2)(p_2 - p_1))\right\}. \tag{52}$$

Similar expressions for $\partial/\partial p_2(\boldsymbol{\nabla}_2 p)^2$ and $\partial/\partial p_3(\boldsymbol{\nabla}_2 p)^2$ are easily obtained by utilizing the symmetry and changing the indices in a cyclic manner.

Introducing the definitions

$$\left\{\begin{array}{c} A_1 \\ A_2 \\ A_3 \end{array}\right\} = \left\{\begin{array}{c} \ell_1^2 - \ell_2^2 - \ell_3^2 \\ \ell_2^2 - \ell_3^2 - \ell_1^2 \\ \ell_3^3 - \ell_1^2 - \ell_2^2 \end{array}\right\} \tag{53}$$

and

$$\left\{\begin{array}{c} \Delta p_1 \\ \Delta p_2 \\ \Delta p_3 \end{array}\right\} = \left\{\begin{array}{c} p_3 - p_2 \\ p_1 - p_3 \\ p_2 - p_1 \end{array}\right\}, \qquad \text{(Note that } \Delta p_1 + \Delta p_2 + \Delta p_3 = 0.\text{)} \tag{54}$$

we get

$$\left\{\begin{array}{c} \frac{\partial}{\partial p_1} \\ \frac{\partial}{\partial p_2} \\ \frac{\partial}{\partial p_3} \end{array}\right\}(\boldsymbol{\nabla}_2 p)^2 = \frac{1}{4A^2}\left\{\begin{array}{c} -A_2\Delta p_2 + A_3\Delta p_3 \\ -A_3\Delta p_3 + A_1\Delta p_1 \\ -A_1\Delta p_1 + A_2\Delta p_2 \end{array}\right\}. \tag{55}$$

Thus,

$$\begin{aligned}\sum_{i=1}^{3}\left\{\frac{\partial}{\partial p_i}(\boldsymbol{\nabla}_2 p)^2\right\}^2 &= \frac{1}{8A^4}\left\{A_1^2{\Delta p_1}^2 + A_2^2{\Delta p_2}^2 + A_3^2{\Delta p_3}^2\right. \\ &\left. - A_2A_3\Delta p_2\Delta p_3 - A_3A_1\Delta p_3\Delta p_1 - A_1A_2\Delta p_1\Delta p_2\right\}. \end{aligned} \tag{56}$$

The error of the magnitude $G = |\,\boldsymbol{G}|$ of the geostrophic wind speed becomes

$$\delta[G] = \frac{\delta[p]}{2\rho f\boldsymbol{\nabla}_2 p}\sqrt{\sum_{i=1}^{3}\left\{\frac{\partial}{\partial p_i}(\boldsymbol{\nabla}_2 p)^2\right\}^2}. \tag{57}$$

With the purpose of reducing systematic errors when dealing with observation, all the equations are made symmetric in (x_1, x_2, x_3), (y_1, y_2, y_3), and (p_1, p_2, p_3).

4 The Thermal Wind

The geostrophic wind velocity given by (34) is under steady, barotropic conditions and the geostrophic wind becomes almost equal to the constant wind velocity aloft.

However, if there are horizontal temperature variations $\boldsymbol{G}$ is not constant with height. A good discussion of this subject has been given by Dutton (1986) who shows that

$$\frac{\partial \boldsymbol{G}}{\partial z} = \frac{g}{fT}\,\boldsymbol{k} \times \boldsymbol{\nabla}_2 T + \frac{1}{T}\frac{\partial T}{\partial z}\,\boldsymbol{G}, \tag{58}$$

where T is the air temperature in °K and g is the acceleration of gravity.

The vertical gradient of $\boldsymbol{G}$ is what is called *the thermal wind*.

Applying (34) and the hydrostatic equation

$$\frac{\partial p}{\partial z} = -\rho g, \tag{59}$$

we may rewrite (58) in the form

$$\frac{\partial \boldsymbol{G}}{\partial z} = \frac{1}{T\rho f}\,\boldsymbol{k} \times \left\{ \frac{\partial T}{\partial z}\boldsymbol{\nabla}_2 p - \frac{\partial p}{\partial z}\boldsymbol{\nabla}_2 T \right\}. \tag{60}$$

Let us for a moment generalize (37) and include the vertical coordinate z, i.e.

$$p = p(x, y, z), \tag{61}$$

and consider the pressure variation around the point (x_0, y_0, z_0).

Locally, the variation δp is given by

$$\delta p = p'_x \delta x + p'_y \delta y + p'_z \delta z, \tag{62}$$

where the derivatives are taken at the point (x_0, y_0, z_0) and where $\delta x = x - x_0$, and $\delta y = y - y_0$, and $\delta z = z - z_0$.

The two-dimensional, constant-pressure surface through (x_0, y_0, z_0) is defined by

$$0 = p'_x \delta x + p'_y \delta y + p'_z \delta z. \tag{63}$$

On this surface the *level line* is defined by $\delta z = 0$, i.e.

$$p'_x \delta x + p'_y \delta y = 0. \tag{64}$$

The unit tangent vector to this line is

$$\boldsymbol{t} = \frac{-p'_y\,\boldsymbol{i} + p'_x\,\boldsymbol{j}}{\sqrt{{p'_x}^2 + {p'_y}^2}}. \tag{65}$$

The normal $\boldsymbol{n}$ to $\boldsymbol{t}$ in the tangent plane is the *principal normal*. It is tangent to the *line of steepest descend* and given by

$$\boldsymbol{n} = \frac{-p'_z p'_x\,\boldsymbol{i} - p'_y p'_z\,\boldsymbol{j} + ({p'_x}^2 + {p'_y}^2)\,\boldsymbol{k}}{\sqrt{{p'_x}^2 + {p'_y}^2}\sqrt{{p'_x}^2 + {p'_y}^2 + {p'_z}^2}}. \tag{66}$$

The normal to the surface, the *binormal vector*, becomes

$$\boldsymbol{b} = \boldsymbol{t} \times \boldsymbol{n} = \frac{p'_x\,\boldsymbol{i} + p'_y\,\boldsymbol{j} + p'_z\,\boldsymbol{k}}{\sqrt{{p'_x}^2 + {p'_y}^2 + {p'_z}^2}} = \frac{\boldsymbol{\nabla}_2 p + \dfrac{\partial p}{\partial z}\,\boldsymbol{k}}{\sqrt{{p'_x}^2 + {p'_y}^2 + {p'_z}^2}}. \tag{67}$$

We can define the analogue unit vectors for the temperature field

$$T = T(x, y, z) \tag{68}$$

as follows

$$\boldsymbol{T} = \frac{-T'_y\,\boldsymbol{i} + T'_x\,\boldsymbol{j}}{\sqrt{{T'_x}^2 + {T'_y}^2}}, \tag{69}$$

$$\boldsymbol{N} = \frac{-T'_z T'_x\,\boldsymbol{i} - T'_y T'_z\,\boldsymbol{j} + ({T'_x}^2 + {T'_y}^2)\,\boldsymbol{k}}{\sqrt{{T'_x}^2 + {T'_y}^2}\sqrt{{T'_x}^2 + {T'_y}^2 + {T'_z}^2}}, \tag{70}$$

and

$$\boldsymbol{B} = \boldsymbol{t} \times \boldsymbol{n} = \frac{T'_x\,\boldsymbol{i} + T'_y\,\boldsymbol{j} + T'_z\,\boldsymbol{k}}{\sqrt{{T'_x}^2 + {T'_y}^2 + {T'_z}^2}} = \frac{\boldsymbol{\nabla}_2 T + \dfrac{\partial T}{\partial z}\,\boldsymbol{k}}{\sqrt{{T'_x}^2 + {T'_y}^2 + {T'_z}^2}}. \tag{71}$$

The necessary and sufficient condition that the two constant-surfaces for p and T coincide locally in the neighborhood of (x_0, y_0, z_0) is that $\boldsymbol{b}$ and $\boldsymbol{B}$ are parallel. According to (67) and (71) this means that in this case

$$\boldsymbol{0} = \boldsymbol{B} \times \boldsymbol{b} = \frac{\boldsymbol{k} \times \left\{ \dfrac{\partial T}{\partial z}\boldsymbol{\nabla}_2 p - \dfrac{\partial p}{\partial z}\boldsymbol{\nabla}_2 T \right\}}{\sqrt{{T'_x}^2 + {T'_y}^2 + {T'_z}^2}\sqrt{{p'_x}^2 + {p'_y}^2 + {p'_z}^2}}. \tag{72}$$

Comparing this equation and (60), we see that the condition that the thermal wind is zero is that the constant-pressure surface and the constant-temperature surface coincide. When (72) is fulfilled we say that we have *barotropic* stratification and *baroclinic* stratification when this is not the case.

Dutton (1986) discussed (58) and found that the second term is about two orders of magnitude smaller than the first. Consequently, we will use the approximation

$$\frac{\partial \boldsymbol{G}}{\partial z} = \frac{g}{fT}\,\boldsymbol{k} \times \boldsymbol{\nabla}_2 T \tag{73}$$

henceforth.

5 The Gradient Wind

The previous considerations have been based on the pressure gradients and not on the second derivatives. This implies that all isobars of p are considered straight. The geostrophic balance means in this case that the vector sum of the horizontal pressure gradient and the Coriolis force is zero. If we want to consider the curvature of the isobars and include the second derivatives, the centrifugal force also enters in the balance. In order to study this we generalize (38):

$$p(x, y) = p_0 + p'_x x + p'_y y + \frac{1}{2}\left\{ p''_{xx} x^2 + 2p''_{xy} xy + p''_{yy} y^2 \right\}. \tag{74}$$

The surface described by (74) is a so-called *quadric surface*. The tangent plane is in general horizontal in exactly one point (x_0, y_0) and this point will be either a maximum point, 'a high', a minimum point, 'a low', or a saddle point surrounded by two high and two low pressure domains. This is determined by signs of the eigenvalues p''_+ and p''_- of the symmetric tensor

$$P'' = \left\{ \begin{array}{cc} p''_{xx} & p''_{xy} \\ p''_{xy} & p''_{yy} \end{array} \right\}. \tag{75}$$

When are p''_+ and p''_- are both positive/negative the surface has a minimum/maximum. When p''_+ and p''_- have opposite signs the surface has a saddle point. There is of course the possibility that one, p''_- say, is zero. In this case the surface is a 'trough' (low pressure, $p''_+ > 0$) or a 'ridge' (high pressure). When both p''_+ and p''_- are zero the surface is a plane.

The determinant of the tensor (75) is equal to the product of p''_+ and p''_-, i.e.

$$p''_+ \times p''_- = \left| \begin{array}{cc} p''_{xx} & p''_{xy} \\ p''_{xy} & p''_{yy} \end{array} \right| = p''_{xx} p''_{yy} - {p''_{xy}}^2 \tag{76}$$

and can be used as a diagnostic tool.

The position (x_0, y_0) of the extremum is determined by setting the first derivatives of (74) equal to zero. This leads to the linear equations

$$\left\{ \begin{array}{cc} p''_{xx} & p''_{xy} \\ p''_{xy} & p''_{yy} \end{array} \right\} \left\{ \begin{array}{c} x_0 \\ y_0 \end{array} \right\} = - \left\{ \begin{array}{c} p'_x \\ p'_y \end{array} \right\} \tag{77}$$

with the solution

$$\left\{ \begin{array}{c} x_0 \\ y_0 \end{array} \right\} = \frac{1}{p''_{xx} p''_{yy} - {p''_{xy}}^2} \left\{ \begin{array}{c} p''_{xy} p'_y - p''_{yy} p'_x \\ p''_{xy} p'_x - p''_{xx} p'_y \end{array} \right\}. \tag{78}$$

The differential equation for the isobars is

$$p'_x \mathrm{d}x + p'_y \mathrm{d}y = 0. \tag{79}$$

Let us follow a Lagrangian particle along the isobar going through the center. Its position $(x(t), y(t))$ in parametric form with time t as parameter must obey

$$(\dot{x}, \dot{y}) \equiv \left(\frac{\mathrm{d}x}{\mathrm{d}t}, \frac{\mathrm{d}y}{\mathrm{d}t} \right) = \frac{1}{\rho f} \left(-p'_y, p'_x \right). \tag{80}$$

We really want to determine the radius of curvature

$$R = \frac{\left(\dot{x}^2 + \dot{y}^2 \right)^{3/2}}{\left| \begin{array}{cc} \dot{x} & \dot{y} \\ \ddot{x} & \ddot{y} \end{array} \right|}. \tag{81}$$

The second derivatives become

$$\ddot{x} = \frac{1}{\rho f} \frac{\mathrm{d}}{\mathrm{d}t} \left(-p'_y \right) = \frac{1}{\rho f} \left\{ -p''_{xy} \dot{x} - p''_{yy} \dot{y} \right\} = \frac{1}{\rho^2 f^2} \left\{ p''_{xy} p'_y - p''_{yy} p'_x \right\} \tag{82}$$

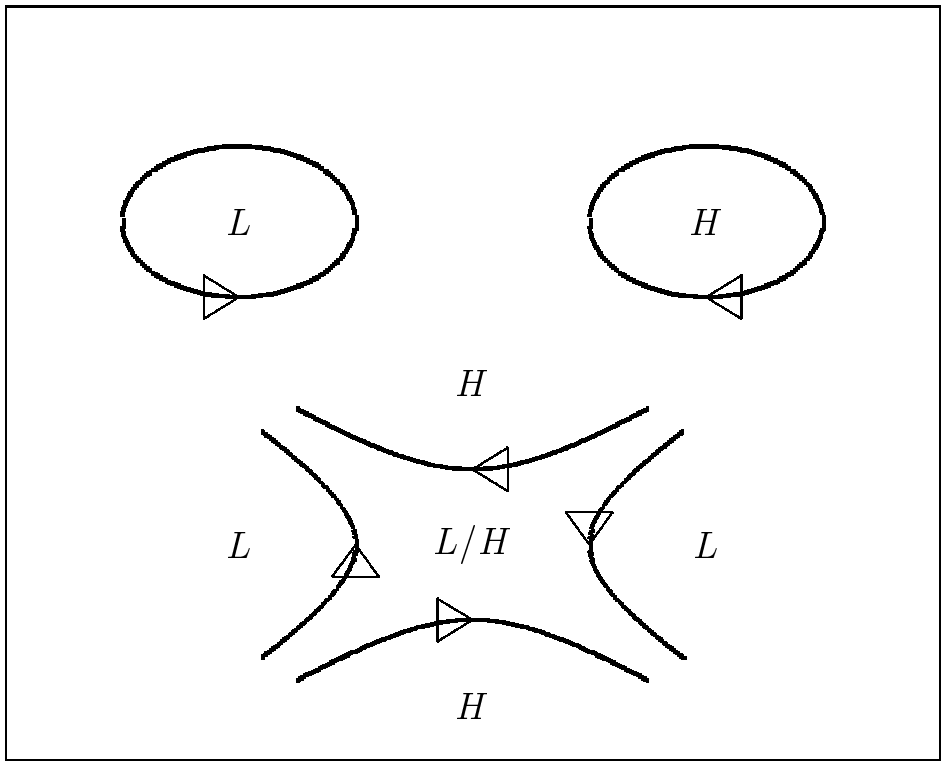

Figure 4. Symbolic representation, by means of isobars of a low-pressure system, a high-pressure system and a saddle point. When there is no horizontal density gradient the air moves along the isobars, clockwise around a low and counterclockwise around a high.

and, similarly,

$$\ddot{y} = \frac{1}{\rho^2 f^2} \left\{ p''_{xy} p'_x - p''_{xx} p'_y \right\}. \tag{83}$$

Inserting in (81) we obtain

$$R = \frac{\left({p'_x}^2 + {p'_y}^2 \right)^{3/2}}{p''_{yy} {p'_x}^2 - 2 p''_{xy} p'_x p'_y + p''_{xx} {p'_y}^2}. \tag{84}$$

If R is not infinite the isobars have curvature, positive around a low pressure and negative around a high pressure. When R is infinite (large compared to the linear dimensions of Denmark) we consider the isobars straight and the pressure surface a plane. In this case geostrophic balance means that the wind aloft has the magnitude and the direction of the geostrophic wind. When the isobars are curved the magnitude of the wind speed aloft is equal to the gradient wind $\mathcal{G}$. The relation between $\mathcal{G}$ and G is given by (Dutton 1986)

$$\frac{G}{fR} \left(\frac{\mathcal{G}}{G} \right)^2 + \frac{\mathcal{G}}{G} - 1 = 0. \tag{85}$$

This equation represents a balance between the centrifugal force $\mathcal{G}^2/R$, the Coriolis force $f\mathcal{G}$, and the pressure force fG.

We see that the important parameter is the dimensionless quantity

$$\frac{G}{fR} = \frac{1}{\rho f^2} \frac{p''_{yy} {p'_x}^2 - 2p''_{xy} p'_x p'_y + p''_{xx} {p'_y}^2}{{p'_x}^2 + {p'_y}^2}. \tag{86}$$

As (85) shows, this parameter, the so-called *Gradient Rossby Number* (Dutton 1986), determines whether or not $\mathcal{G}$ and G are approximately equal. Solving (85) for $\mathcal{G}/G$, we get only one meaningful solution (see Fig. 5):

$$\frac{\mathcal{G}}{G} = \frac{-1 + \sqrt{1 + 4G/(fR)}}{2G/(fR)}. \tag{87}$$

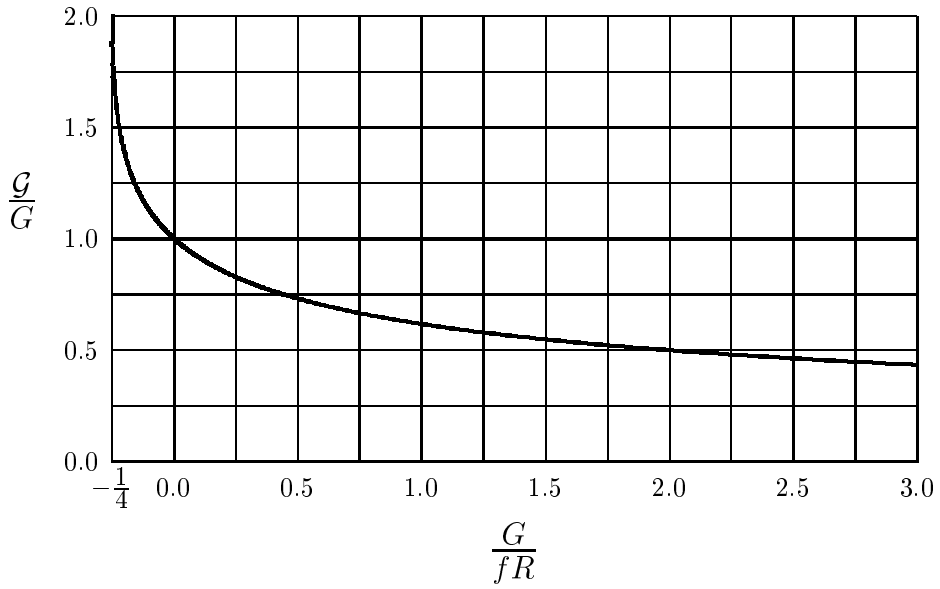

Figure 5. The solution to (87).

If $G/(fR)$ is small compared to one we get, by expanding the square root

$$\frac{\mathcal{G}}{G} = 1 - \frac{G}{fR} + O\left(\left\{\frac{G}{fR}\right\}^2\right) \approx 1 - \frac{G}{fR}. \tag{88}$$

The balance (85) cannot be maintained when $G/(fR) < -1/4$.

6 The Surface Wind

At the Earth's surface the Coriolis force is of no importance and the resistance force from the surface becomes dominant. When the terrain is horizontally homogeneous with a roughness length z_0 the variation close to the surface of the wind speed with height z is under neutral conditions given by

$$U(z) = \frac{u_*}{\kappa} \ln\left(\frac{z}{z_0}\right), \tag{89}$$

where $\kappa \simeq 0.4$ is the von Kármán constant and u_* the friction velocity.

In this idealized situation it is possible to establish a connection between the magnitude and direction of the geostrophic wind and those of the surface wind. An elegant derivation of this relation, *the geostrophic drag law*, is given by Tennekes & Lumley (1978). If the angle from the direction of the geostrophic wind to that of the surface wind is α then

$$G\cos\alpha = \frac{u_*}{\kappa}\left\{\ln\left(\frac{u_*}{fz_0}\right) - A\right\} \tag{90}$$

$$G\sin\alpha = \frac{u_*}{\kappa}B, \tag{91}$$

where A and B are dimensionless constants. There is a considerable uncertainty about what the best values of these constants. Since they are based on the logarithmic wind profile (89), pertaining to a neutral stratification of the surface layer, an experimental determination of A and B must be carried out under conditions with strong surface winds. Even then there does not seem to be a general agreement as to what values should be used. Tennekes & Lumley (1978) and Mortensen et al. (1993) and others use $A = 1.8$ and $B = 4.5$ whereas Panofsky & Dutton (1984) suggest $A \simeq 0$ and $B \simeq 5$ for strong winds.

The two equations (90) and (91) may be recast in the form

$$G = \frac{u_*}{\kappa}\sqrt{\left\{\ln\left(\frac{u_*}{fz_0}\right) - A\right\}^2 + B^2} \tag{92}$$

and

$$\alpha = \arctan2\left(\ln\left(\frac{u_*}{fz_0}\right) - A, B\right). \tag{93}$$

We see that if the geostrophic wind velocity $\boldsymbol{G}$ is known, i.e. both magnitude and direction, then the magnitude and direction of the surface wind can be calculated at a given latitude (for the determination of f) and for a given roughness length z_0 by first solving (92) for u_* and inserting in (89) and, subsequently, by using (93) to calculate the turning of the wind α from the geostrophic wind to the surface wind.

Figure 6 shows schematically the relation between G, U and α.

7 Data and Data Analysis

The data from each station is stored year by year as an ASCII file with a name which includes information about the name of the station and the year. The form is "p_nam_ye.dat", where "p" shows that it is a pressure file, where "nam" stands for the first three letter of the name of the station[†], and where "ye" is the last two digits of the year. For example the pressure data from Risø from 1998 are stored in the file "p_ris_98.dat".

The files are formatted as records, where numbers are separated by space, and where

[†]The Danish letters "æ", "ø", and "å" will here be replaced by "a", "o", and "aa", respectively.

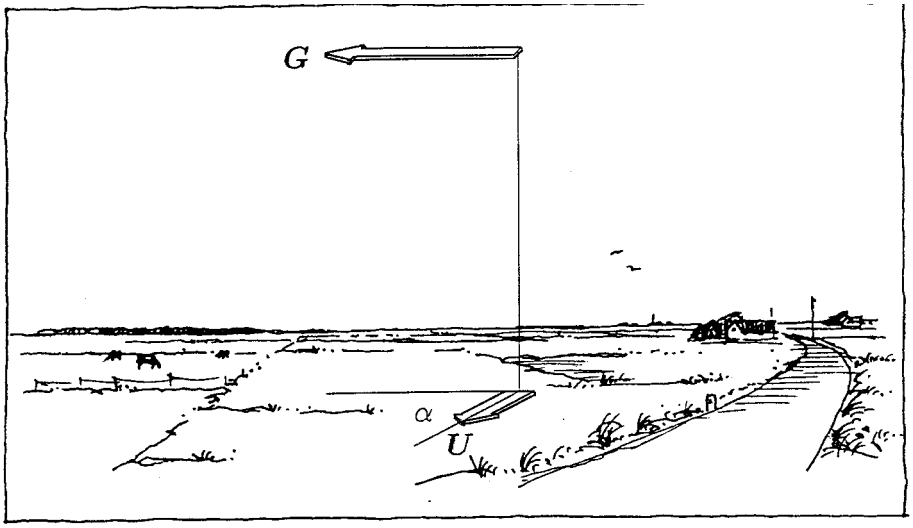

Figure 6. Schematics of the relations between the geostrophic wind G, the surface wind U, and the angle α between them.

the first holds the latitude in degrees, minutes, and seconds,

the second record the longitude in degrees, minutes, and seconds,

the third the altitudes in m, and

each of the following the pressure at the observation altitude, the air temperature in °C, the year with all four digits, and the month, day, hour, and minute in the form "MODAHOMI".

The pressure records used in the following analysis cover the periods given in Table 2.

Table 2. Timetable for pressure measurements.

	Start			Stop		
Ulborg	1998	0429	13:45	1999	0606	23:55
Børglum	1998	0429	13:45	1999	0606	23:55
Kegnæs	1998	0429	13:45	1999	0606	23:55
Balle	1998	0429	13:45	1999	0323	10:25
Gedser	1998	0429	13:45	1999	0627	09:55
Risø	1998	0429	13:45	1999	0606	23:55

As explained in section 3 we may calculate the geostrophic wind speed and direction from three barometer stations.

The software has been developed and Table 3 shows a sample output. The top consists of various household data, such as the name and version of the program

used, ellipsoid data, geographical positions in decimal degrees of the three stations and that of their center of mass, the altitudes of the three stations, and the Coriolis parameter pertaining to the center of mass position. In the main body of the table are the pressures, reduced to sea level, the temperatures in °C, the geostrophic wind speed G, the error $\delta[G]$ according to (57), the geostrophic wind direction, the magnitude and direction of the thermal wind, and the observation time.

Table 3. Sample output from the stations Risø, Kegnæs, and Gedser.

```
#Source code: C:\LKDOC\GSTR\TYST_A_B\G_WIND08.PAS. Time stamp: 3 November 1999, 15:29.
#
#Pressure and temperature
#
#Semimajor axis (datum ED50): 6378.388 km.
#Eccentricity (datum ED50): 0.08199189045.
#
#Site    Latitude Longitude Altitude
#==================================
#Kegnaes  54.8557    9.9363   7.45
#Gedser   54.5697   11.9429   2.28
#Risoe    55.6948   12.0895   8.04
#mean pos 55.0445   11.3190
#Coriolis parameter: 0.0001195319
#
#Year: 1998.
#
#Distances:
#Gedser   - Risoe   : 125.611 km
#Risoe    - Kegnaes : 165.696 km
#Kegnaes  - Gedser  : 133.192 km
#
#    Kegnaes       Gedser          Risoe       G    errG   dirG   ThW  dirThW YEAR MO DA HO MI
#   mb     C      mb     C      mb     C     m/s    m/s   deg    s^(-1) deg
#=============================================================================================
#
 1009.81  10.1 1008.76   8.3 1009.95  14.4   7.69   0.83  60.4   0.014  88.1 1998 04 29 13 45
 1009.81  10.2 1008.70   9.3 1010.04  14.6   8.48   0.84  62.5   0.012  94.9 1998 04 29 13 55
 1009.71  10.2 1008.62   9.3 1010.31  14.4   9.91   0.83  70.2   0.012  94.6 1998 04 29 14 05
 1009.71  10.2 1008.54   9.1 1010.23  14.3  10.08   0.83  68.1   0.012  92.6 1998 04 29 14 15
 1009.71  10.2 1008.48   9.0 1010.07  14.7   9.83   0.83  64.7   0.013  92.7 1998 04 29 14 25
 1009.71  10.2 1008.41   8.7 1009.95  15.3   9.80   0.84  61.8   0.015  91.8 1998 04 29 14 35
```

7.1 Geostrophic Climatology

We can now determine the geostrophic wind by means of three stations as shown in section 3. We have chosen 10 such triangles of stations to investigate a possible geographical variation of the geostrophic wind climate. Figure 7 shows the positions of the centers of these triangles and Table 4 their geographical positions.

We have calculated time series of the geostrophic wind speed G and direction D_G as 10 minute averages for all ten centers. These records in their the entire lengths have been used to determine for each center the mean $\langle G \rangle$, the mean square $\langle G^2 \rangle$ and histograms of G in twelve 30° sectors, centered around $000°, 030°, \ldots, 330°$ and for all directions. Under the assumption that the probability density function

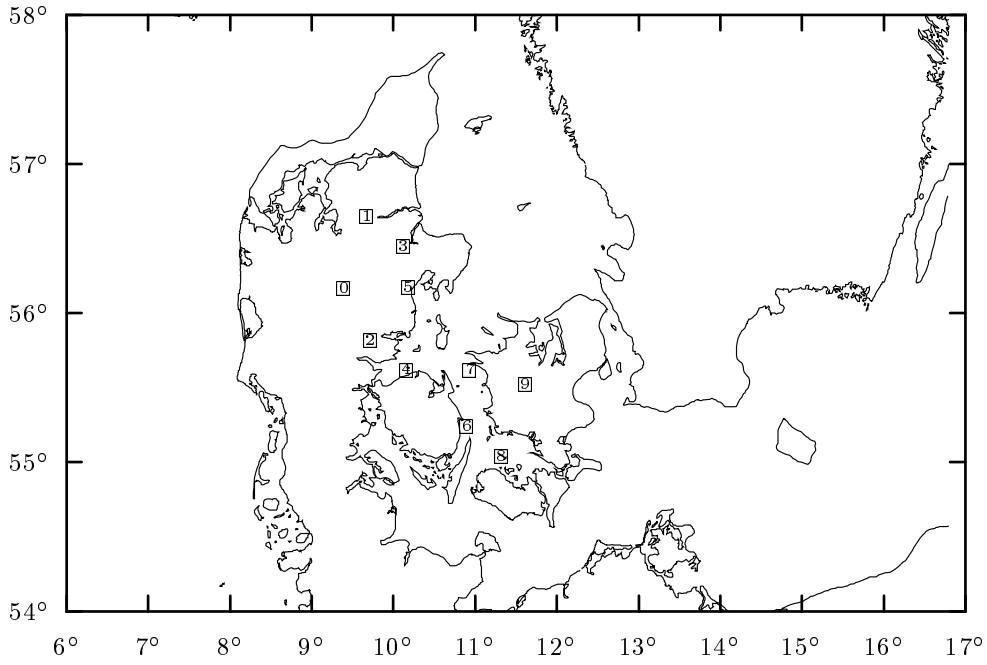

Figure 7. Center positions for the 10 triangles, numbered from 0 to 9.

Table 4. Positions of the ten centers. The positions are given in the datum ED50.

No	Center	Triangle			Longitude	Latitude
0	BOULKE	Børglum	Ulborg	Kegnæs	09°23′40″	56°10′05″
1	BOULBA	Børglum	Ulborg	Balle	09°40′34″	56°39′14″
2	ULKEBA	Ulborg	Kegnæs	Balle	09°43′19″	55°49′24″
3	BOULRI	Børglum	Ulborg	Risø	10°13′20″	56°27′18″
4	ULKERI	Ulborg	Kegnæs	Risø	10°09′30″	55°37′26″
5	BOKEBA	Børglum	Kegnæs	Balle	10°10′50″	56°10′22″
6	BAKEGE	Balle	Kegnæs	Gedser	10°53′41″	55°14′55″
7	BAKERI	Balle	Kegnæs	Risø	10°56′01″	55°37′26″
8	KEGERI	Kegnæs	Gedser	Risø	11°19′08″	55°02′42″
9	BAGERI	Balle	Gedser	Risø	11°36′58″	55°31′36″

of G is well represented by the Weibull distribution

$$p(G) = \frac{k}{\mathcal{A}} \left(\frac{G}{\mathcal{A}}\right)^{k-1} \exp\left(-\left[\frac{G}{\mathcal{A}}\right]^{k}\right), \tag{94}$$

$\langle G \rangle$ and $\langle G^2 \rangle$ have been used to determine the parameters $\mathcal{A}$ and k.

At all the centers, except at ULKERI (4) and at BAGERI (9), the highest value of G was found in the 300° sector. The mean $\langle G_{300^\circ} \rangle$ for this sector and for all directions are given in Table 5.

Table 5. Maximum, mean and mean in the 300° *sector of* G.

No	Center	max G	D_G	Time			$\langle G \rangle$	$\langle G_{300^\circ} \rangle$
0	BOULKE	59.8 m/s	196°	1998	0714	10:25	11.9±0.1 m/s	14.9±0.2 m/s
1	BOULBA	52.8 m/s	295°	1999	0125	15:35	12.0±0.1 m/s	15.8±0.2 m/s
2	ULKEBA	46.9 m/s	219°	1998	0714	10:25	11.5±0.1 m/s	14.1±0.2 m/s
3	BOULRI	54.4 m/s	289°	1999	0125	15:35	11.7±0.1 m/s	15.1±0.2 m/s
4	ULKERI	44.6 m/s	230°	1998	0714	10:25	10.6±0.1 m/s	12.3±0.2 m/s
5	BOKEBA	47.8 m/s	310°	1998	1025	23:55	12.1±0.1 m/s	14.2±0.2 m/s
6	BAKEGE	46.3 m/s	273°	1998	1025	23:15	11.2±0.1 m/s	13.4±0.2 m/s
7	BAKERI	53.1 m/s	256°	1998	1025	23:15	11.7±0.1 m/s	13.2±0.2 m/s
8	KEGERI	39.9 m/s	215°	1998	1028	07:05	10.6±0.1 m/s	12.9±0.2 m/s
9	BAGERI	45.5 m/s	355°	1998	1106	11:05	11.7±0.1 m/s	13.2±0.2 m/s

Table 6 is a list of the Weibull parameters, $(k, \mathcal{A})$ for all directions and $(k_{300^\circ}, \mathcal{A}_{300^\circ})$ for $D_G = 300^\circ$ and Figure 8 shows as an example the frequency distributions of G for all directions and for the 300° sector. The complete information about all the Weibull parameters can be found in the appendix.

At each of the centers listed in Table 4 the maximum value of G was selected, together the corresponding direction and the time of occurrence, for a preliminary investigation of extreme events. Only data from before March 19, 1999, where there was a major interruption in the data recording in Balle, were used.

Each of the ten maximum values of G were compared to the simultaneous values of G at the nine other centers. Several of the maximum values of G were simultaneous. Further, the data from Ulborg were periodically interrupted for rather long durations. The result is that, with this selection criteria, we have found only three events where *all* the centers provide relevant data. The results are listed in Table 7 and shown in Figs. 9, 10, and 11.

Table 6. Weibull parameters.

No	Center	k	$\mathcal{A}$	k_{300°	$\mathcal{A}_{300^\circ}$
0	BOULKE	1.86	13.4 m/s	2.05	16.8 m/s
1	BOULBA	1.90	13.5 m/s	2.18	17.9 m/s
2	ULKEBA	1.90	13.0 m/s	2.16	15.9 m/s
3	BOULRI	1.87	13.2 m/s	2.09	17.0 m/s
4	ULKERI	1.92	11.9 m/s	2.16	13.9 m/s
5	BOKEBA	2.03	13.6 m/s	2.15	16.0 m/s
6	BAKEGE	1.90	12.7 m/s	2.21	15.1 m/s
7	BAKERI	1.91	13.2 m/s	2.27	14.9 m/s
8	KEGERI	1.88	11.9 m/s	2.00	14.6 m/s
9	BAGERI	1.93	13.2 m/s	2.09	14.9 m/s

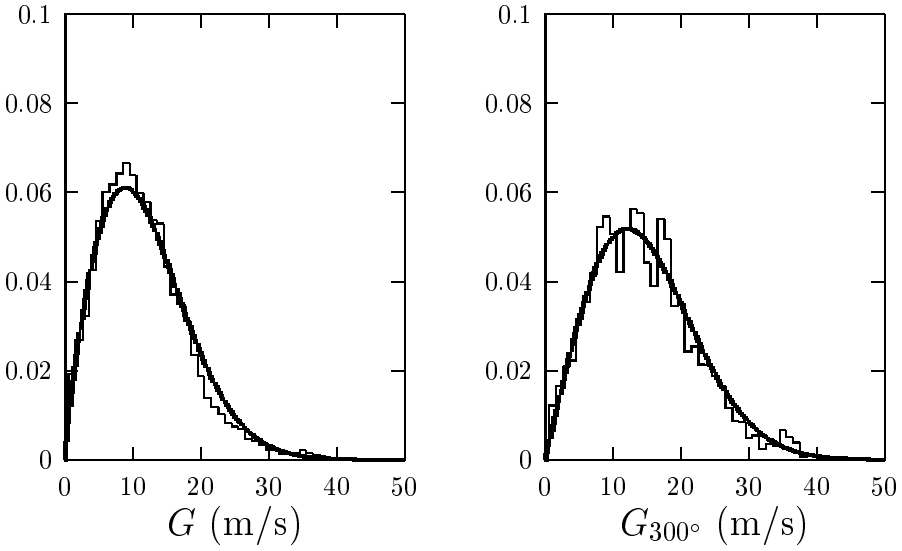

Figure 8. Histograms and corresponding Weibull distributions for all directions (left frame) and for the 300° *sector (right frame) at center number 0, BOULKE.*

It is not safe to draw too definite conclusions from these time limited records of the geostrophic wind velocities. Further, not all the ten centers are equally well suited for analyzing the geostrophic wind field. In fact, by comparing Figs. 7 and 10, we see that three of them, BOULKE (0), BOKEBA (5), and BAGERI (9), are rather 'shallow'.

Even then the results above seem to indicate that:

Table 7. Three events where at least one center has its maximum value of G.

		1998 0714 10:25		1998 1028 07:05		1999 0125 15:35	
No	Center	G	D_G	G	D_G	G	D_G
0	BOULKE	59.8 m/s	196°	08.7 m/s	347°	53.1 m/s	318°
1	BOULBA	36.0 m/s	183°	10.8 m/s	253°	52.8 m/s	295°
2	ULKEBA	46.9 m/s	219°	05.6 m/s	123°	34.3 m/s	311°
3	BOULRI	37.6 m/s	184°	12.4 m/s	248°	54.4 m/s	289°
4	ULKERI	44.6 m/s	230°	14.0 m/s	140°	18.9 m/s	295°
5	BOKEBA	19.1 m/s	258°	20.9 m/s	183°	34.6 m/s	264°
6	BAKEGE	27.9 m/s	236°	37.2 m/s	191°	33.1 m/s	273°
7	BAKERI	33.4 m/s	229°	17.0 m/s	180°	35.2 m/s	263°
8	KEGERI	24.7 m/s	227°	39.9 m/s	215°	28.5 m/s	271°
9	BAGERI	33.2 m/s	214°	20.7 m/s	271°	30.3 m/s	253°

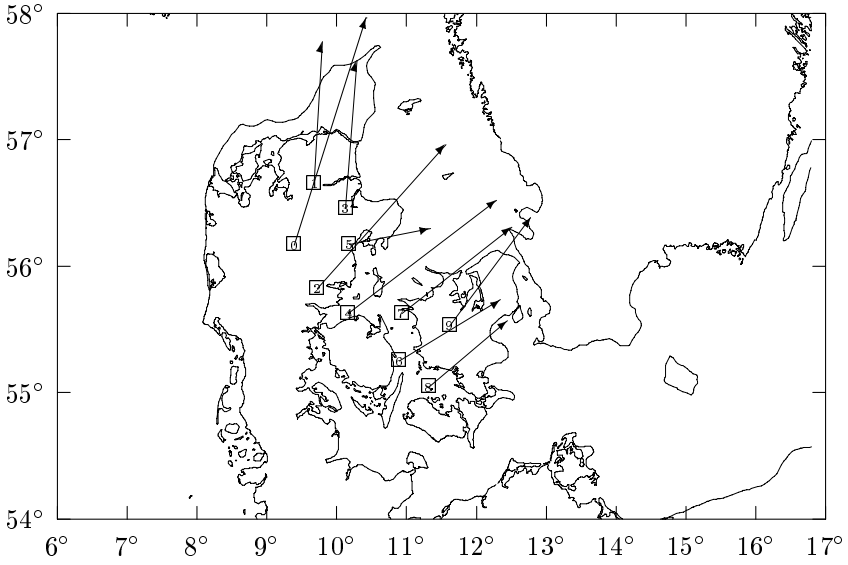

Figure 9. Extreme geostrophic wind speed on July 14, 1998. Centers 0, 2, and 4 have their maximum values on this date.

1. the largest mean values of G are in the 300° direction sector,
2. both $\langle G \rangle$ and $\langle G_{300°} \rangle$ increase in magnitude when going from west to east, and

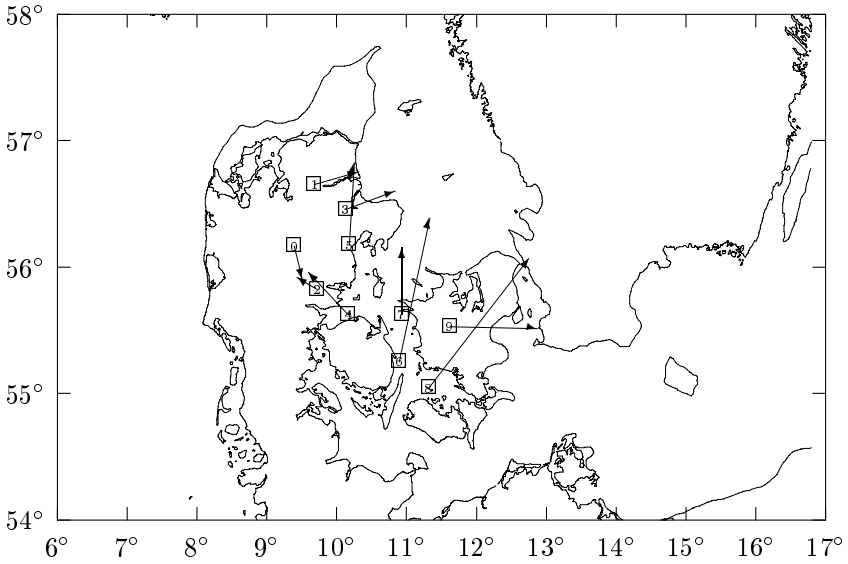

Figure 10. Extreme geostrophic wind speed on October 28, 1998. Center 8 has its maximum value on this date.

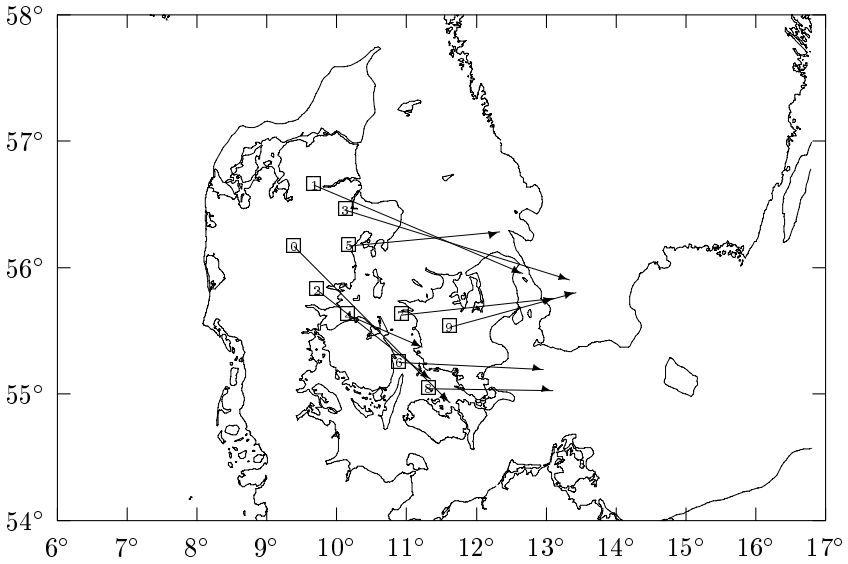

Figure 11. Extreme geostrophic wind speed on January 25, 1999. Centers 1 and 3 have their maximum values on this date.

3. when G is at maximum in the western part of the country the simultaneous values in the eastern part are considerably smaller and not corresponding to the maximum values there.

7.2 Gradient and Geostrophic Wind

In section 5 we discussed the gradient wind $\mathcal{G}$ where the curvature of the isobars is taken into account by including the centrifugal force in the balance with the horizontal pressure gradient and the Coriolis force. We are actually able to determine this curvature from the six pressure observations since there are exactly six unknown constants in the quadric surface described by (74).

The curvature of isobars may also result in a different estimate of the geostrophic wind speed G_6 compared to that obtained from three pressure observations G_3 where the isobars are assumed to be straight. The directions corresponding to G_6 and $\mathcal{G}$ however, are the same. We have carried out a comparison between G_3, G_6, and $\mathcal{G}$ and center number 8 (KEGERI). Figure 12 shows these three speeds, the Gradient Rossby Number, and the directions for a short period of three days and Figs. 13, 14, 15 more complete comparisons between G_6 and G_3, $\mathcal{G}$ and G_3, and D_{G_6} and D_{G_3}, respectively.

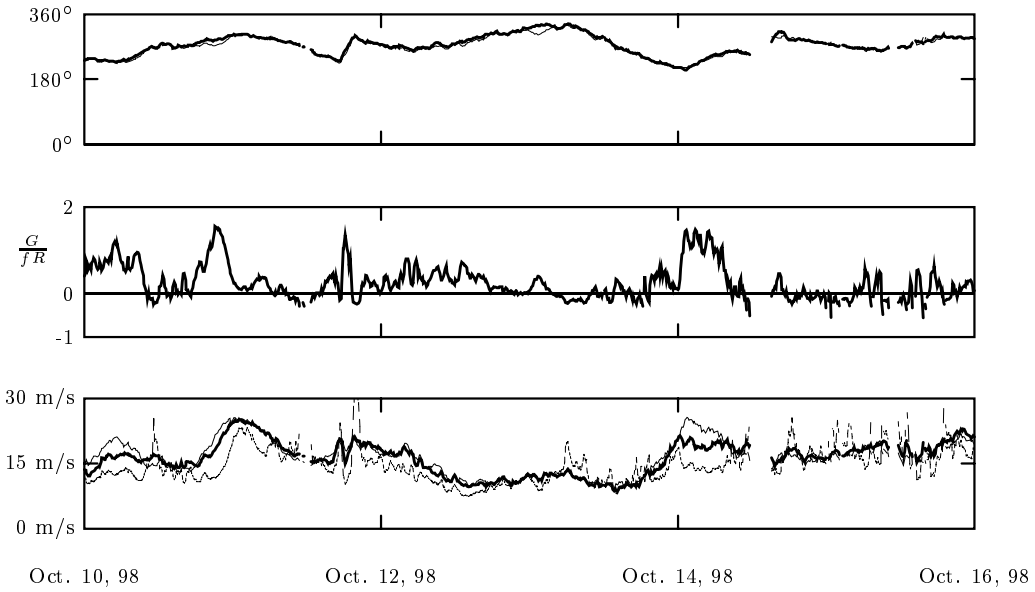

Figure 12. Lower frame: G_6 (thick line), G_3 (thin line), and $\mathcal{G}$ (dashed line). Middle frame: $G/(fR)$. Top frame: direction of the geostrophic wind from three pressure measurements (thick line) and from six pressure measurements (thin line). Data from center number 8 (KEGERI).

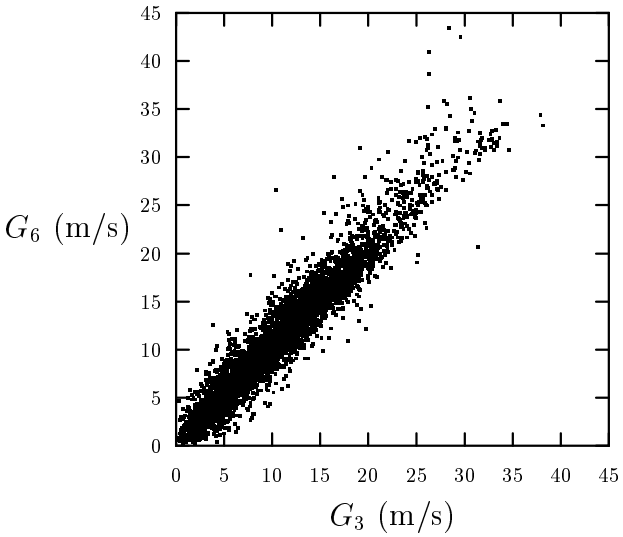

Figure 13. Comparison between the geostrophic wind speed based on six simultaneous pressure observations and that based on three at center number 8 (KEGERI).

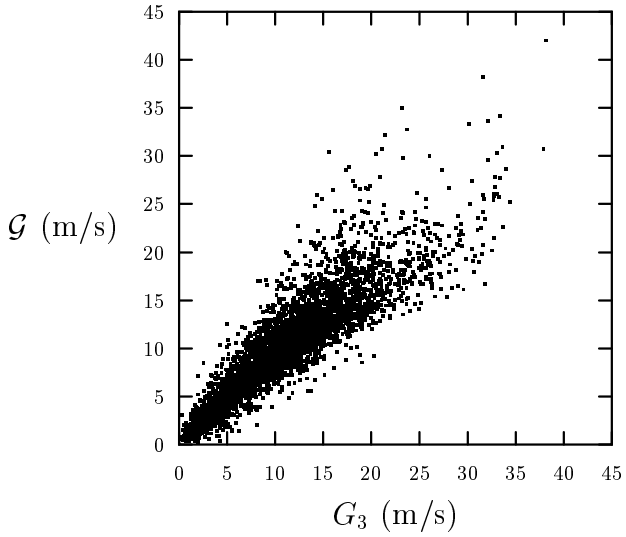

Figure 14. Comparison between the gradient wind speed and the geostrophic wind at center number 8 (KEGERI) based on three simultaneous pressure observations.

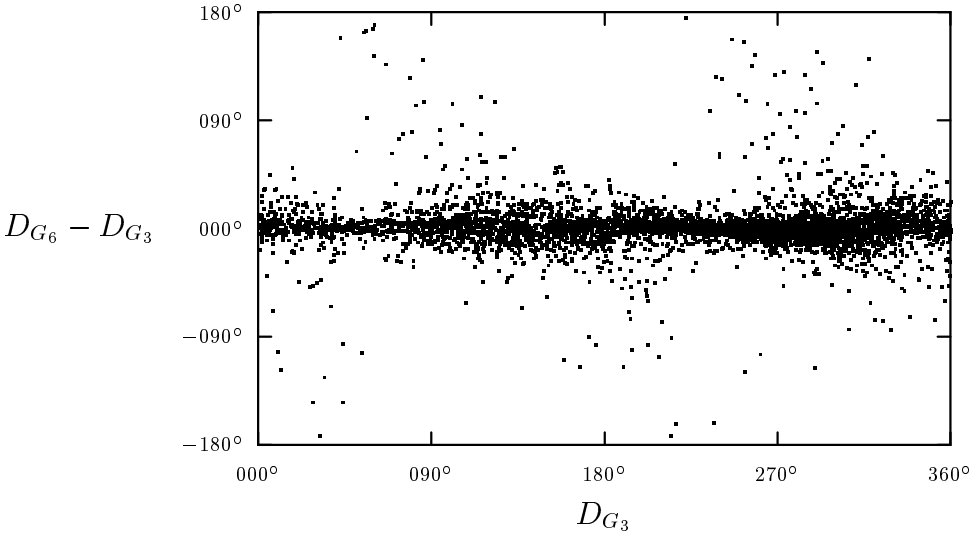

Figure 15. The difference between the direction of the geostrophic wind based on six stations and that based on three stations at center number 8 (KEGERI).

Figure 12 seems to show that G_6 tracks G_3 quite well and also that there is good agreement between the directions D_{G_6} and D_{G_3}. The gradient wind $\mathcal{G}$ is usually somewhat lower than the geostrophic wind which of course is no surprise (see Fig. 5) when observing that the middle frame shows that the Gradient Rossby Number is nearly always positive, corresponding to low-pressure situations. The few times this number is negative the gradient wind is larger than the geostrophic wind.

Figures 13, 14, and 15 is an indication of how large deviations one must expect when comparing velocities and directions obtained in different ways.

7.3 Review of the Geostrophic Drag Law

It is possible to compare the geostrophic wind and the measured surface wind at Tystofte. Ten minute averages of wind speed and direction has been contiguously recorded at the top of a 39.3 m mast since May 25, 1982. Its geographical coordinates are $(\lambda, \varphi) = (11°19'48'', 55°14'24'')$, i.e. about 23 km straight north of the center KEGERI (8). Kristensen et al. (1999) discuss these data and show how WA^{S}P (Mortensen et al. 1993) can be used to determine, for a given measured wind speed, the friction velocity u_* for any direction of the wind. Consequently, we have simultaneous records of the geostrophic wind and the surface wind and should be able to determine the dimensionless constants A and B in the geostrophic drag law (90) and (91).

We expect A and B to depend on the stability of the atmospheric surface layer (Tennekes 1982). We are mostly interested in strong winds where the flux of specific momentum is dominating, i.e. where the thermal stratification can be considered close to neutral. We have consequently excluded, somewhat arbitrarily, situations where u_* is smaller than 0.4 m/s. According to (89), this value of u_* corresponds to a wind speed of about 5 m/s at 10 m over a terrain with the roughness length $z_0 = 0.05$ m/s. The values A and B, obtained from the data, showed a considerable scatter. Figure 16 shows a histogram and a Gaussian fit to the data.

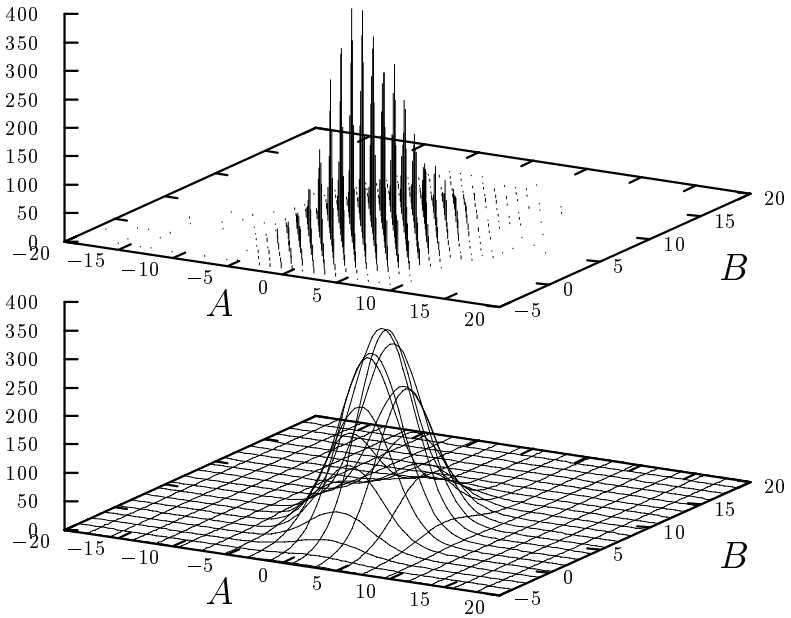

Figure 16. Two-dimensional histogram and Gaussian fit to A and B, obtained from the Tystofte wind data and the simultaneous pressure observations at Kegnæs, Gedser, and Risø. The mean values, the standard deviations, and the correlation coefficient are $(\langle A\rangle, \langle B\rangle) = (0.8, 4.1)$, $(\sigma_A, \sigma_B) = (2.9, 2.9)$, *and* $\rho_{AB} = -0.16$, *respectively.*

To test to what extent A and B depend on u_* we have also calculated average values of A and B by successively excluding data where u_* is smaller than a certain value. the result is shown in Fig. 17.

As mentioned in 6 recommended values are $0 \lessapprox A \lessapprox 1.8$ and $4.5 \lessapprox B \lessapprox 5$. We find that $A = 0.5$ and $B = 3.5$ are in reasonable agreement with our observations, in particular for higher wind speeds.

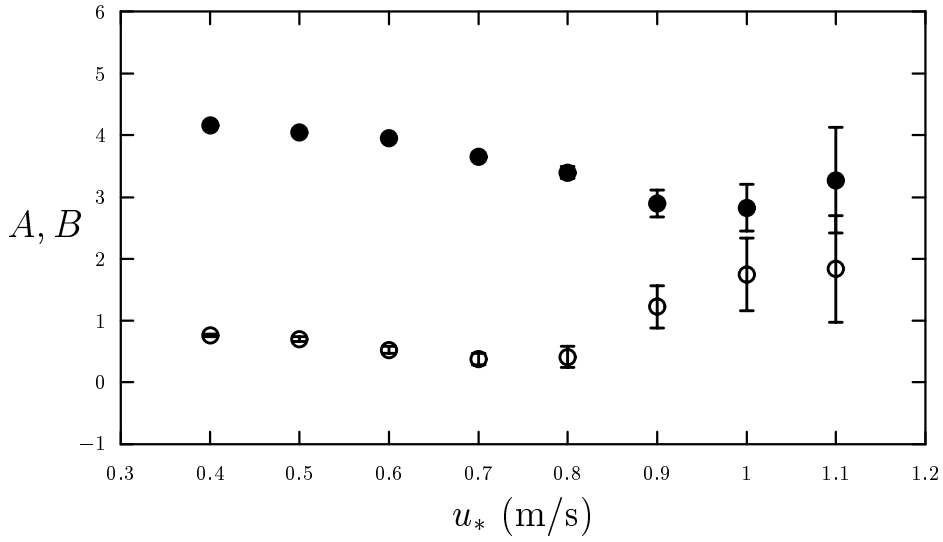

Figure 17. The mean values of A (closed circles) and B (open circles) as functions of the lower value of the friction velocity.

There seems to be a large discrepancy between our findings and those used routinely in e.g. WAsP. However, in some applications this is of limited consequence. For example, if for a given geostrophic wind we want to determine how the friction velocity changes with changing roughness length there is the simple approximate relation (Kristensen et al. 1999)

$$u'_* = u_* \left(\frac{z'_0}{z_0} \right)^q, \tag{95}$$

where the primed variables are the new values of the friction velocity and the roughness length. The exponent q is about 0.069 for $(A, B) = (1.8, 4.5)$ and $0.067 \simeq 1/15$ for $(A, B) = (0.5, 3.5)$. In the first case the friction velocity changes by 17.2% when the roughness length changes by a factor of 10. In the second case the corresponding change i u_* is 16.7%.

To estimate the influence on the relation between the surface wind and the geostrophic wind we rewrite (92) and (93) as

$$\frac{\kappa G}{u_*} = \sqrt{(L - A)^2 + B^2}, \tag{96}$$

and

$$\tan(\alpha) = \frac{B}{L - A}, \tag{97}$$

where

$$L = \ln\left(\frac{u_*}{f z_0} \right) \tag{98}$$

characterizes the magnitude of the surface wind speed in a given terrain with the roughness length z_0 at a given latitude. The range

$$10 < L < 15 \tag{99}$$

covers all situations of practical importance.

If the changes in A and B are δA and δB, respectively, the change in α becomes

$$\delta\alpha = \frac{(L-A)\delta B + B\delta A}{(L-A)^2 + B^2} \approx \frac{\delta B}{L-A} + \frac{B\delta A}{(L-A)^2} \approx \frac{B}{L}\frac{\delta A}{L} + \frac{\delta B}{L}. \tag{100}$$

Since L will then be somewhat larger in magnitude than both A and B, we approximate (96) by a second-order expansion in A/L and B/L.

$$\begin{aligned}
\frac{\kappa G}{u_*} &= \left\{(L-A)^2 + B^2\right\}^{1/2} \\
&= L\left\{1 - 2\frac{A}{L} + \frac{A^2+B^2}{L^2}\right\}^{1/2} \\
&\approx L\left\{1 - \frac{A}{L} + \frac{A^2+B^2}{2L^2} - \frac{1}{8}\left(-2\frac{A}{L}\right)^2\right\} \\
&= L - A + \frac{B^2}{2L}.
\end{aligned} \tag{101}$$

Roughly we have

$$\frac{\delta G}{G} \approx -\frac{\delta A}{L} + \frac{B}{L}\frac{\delta B}{L}. \tag{102}$$

The approximate relations (100) and (102) show that a change in A is more important for G than the same change in B. The opposite is the case for α.

7.4 Comparison with Surface Measurements

We have compared surface wind data with the geostrophic wind at two different sites, using the geostrophic drag laws (92) and (93) with $A = 0.5$ and $B = 3.5$, derived by comparing Tystofte data and data from center number 8 (KEGERI).

First we used the Tystofte data to predict the direction and magnitude of the geostrophic wind and compared with the geostrophic wind at center 8 (KEGERI) which is, within 2°, approximately 22 km due south of Tystofte. Figure 18 shows time series over 10 days of the predicted and the observed direction and magnitude of the geostrophic wind.

It is obvious that the tracking is far from perfect. For example, there seems to be a significant discrepancy between the geostrophic wind speeds on May 13 1998. The directions, however, do not contradict one another. That particular day there is, according to the weather surface map, a high pressure of 1035 HPa about 800 km north of Denmark, where the surface pressure is about 1025 HPa. A possible explanation for the discrepancy is therefore that the gradient wind which is indeed larger than the geostrophic wind should have been compared to the prediction.

Figure 18 also shows that changes in the predicted and the observed geostrophic wind speed do not always occur simultaneously. This is illustrated quite well by the record: late on May 9 1998 the observed geostrophic wind speed precedes the predicted by a couple of hours and 24 hours later the situation is the opposite.

In the first case the geostrophic wind direction is about 180° and in the second between 0° and 90°.

We have used the entire Tystofte and KEGERI records to compare predicted and observed geostrophic wind. The result is shown in Figs. 19 and 20. In both plots there is a large scatter and Fig. 19 shows that the predicted geostrophic wind speed $G_{\text{pred.}}$ in the mean is smaller than the observed $G_{\text{obs.}}$. In fact, a least square fit gives the result $G_{\text{pred.}} \approx 0.7 G_{\text{obs.}} + 3$ m/s.

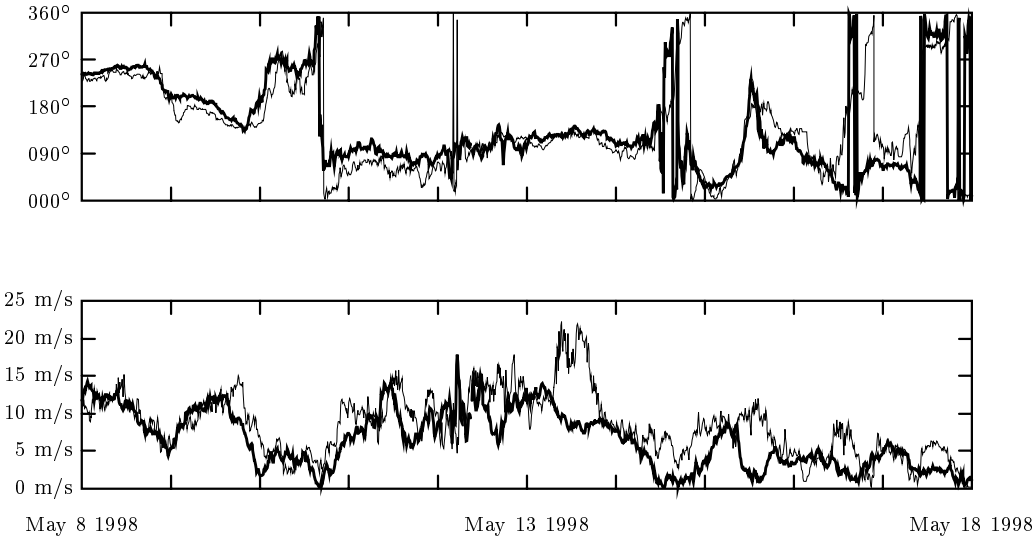

Figure 18. Comparison between predicted (thin line) and observed (thick line) Geostrophic wind at center number 8 (KEGERI). Upper frame: directions. Lower frame: geostrophic wind speeds. The prediction is based on the Tystofte data.

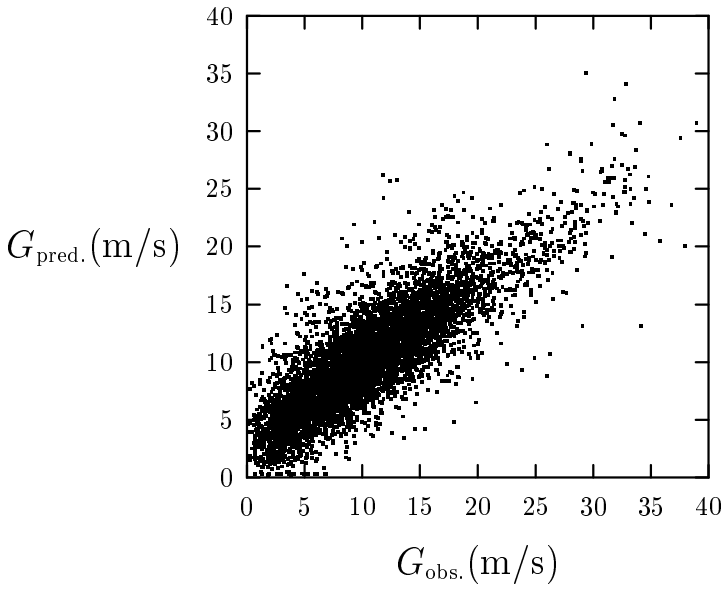

Figure 19. Comparison between the predicted geostrophic wind speed at Tystofte and the observed geostrophic wind at center number 8 (KEGERI).

We have also carried out a more independent test of the geostrophic drag law by using the values of A and B derived from the Tystofte and KEGERI data to

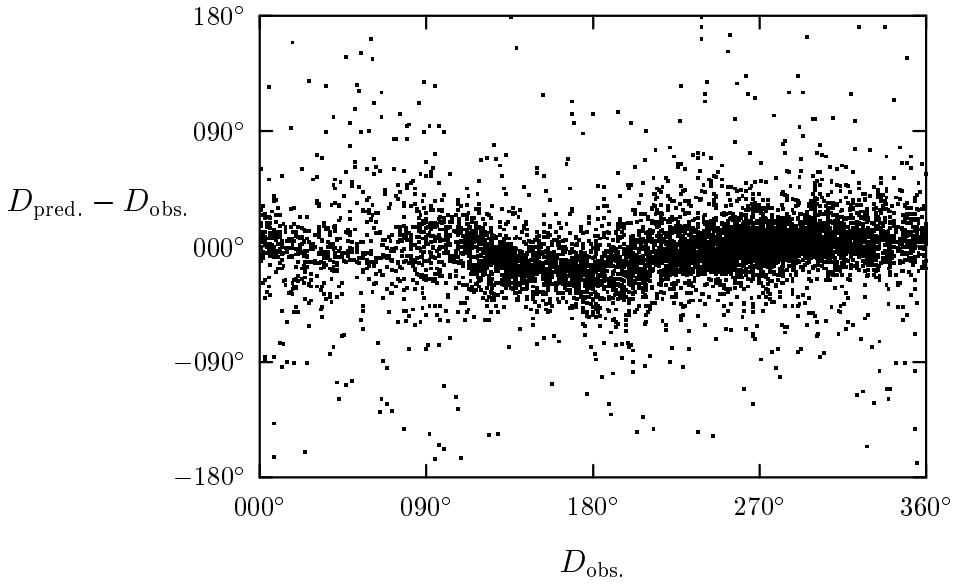

Figure 20. The difference between the predicted and the observed direction of the geostrophic wind based on data from Tystofte and center number 8 (KEGERI).

compare the geostrophic wind at center number 1 (BOULBA) (see Fig. 7) and that predicted by the surface data at Børglum about 78 km to the north (geographical direction 6°). A ten-day record of the prediction and the observation is shown in Fig. 21. This figure shows good agreement at times and also direct disagreement for rather long periods. Using the entire record, we compare magnitudes and directions in Figs. 22 and 23. The scatter is larger than in the corresponding plots Figs. 19 and 20, but here $G_{\text{pred.}}$ does not underpredict $G_{\text{obs.}}$ to the same extent ($G_{\text{pred.}} \approx 0.8G_{\text{obs.}} + 3$ m/s).

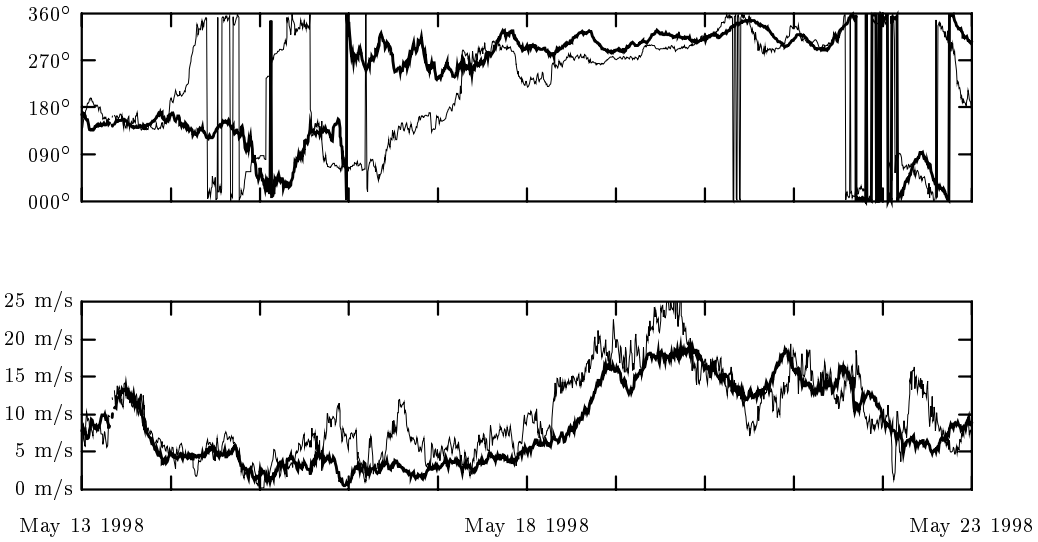

Figure 21. Comparison between predicted (thin line) and observed (thick line) Geostrophic wind at center number 1 (BOULBA). Upper frame: directions. Lower frame: geostrophic wind speeds. The prediction is based on the Børglum data with A and B derived from the Tystofte-KEGERI data.

There are several possible explanations for the less than perfect agreement between

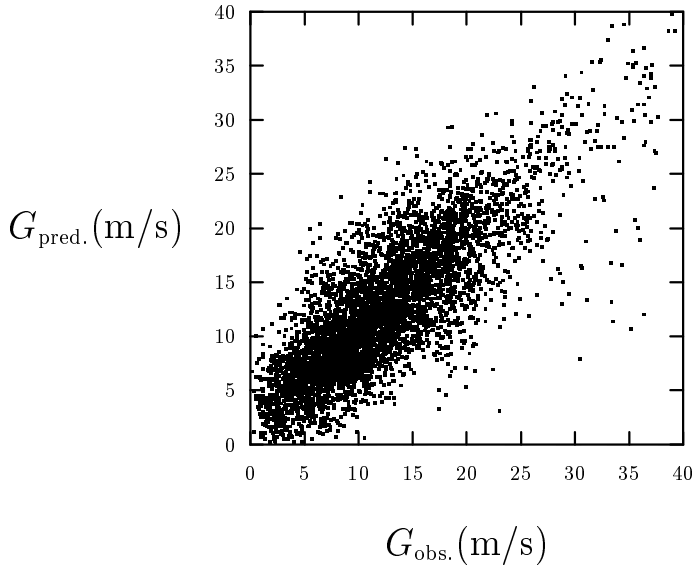

Figure 22. Comparison between the predicted geostrophic wind speed at Børglum, using A and B from the Tystofte-KEGERI data, and the observed geostrophic wind at center number 1 (BOULBA).

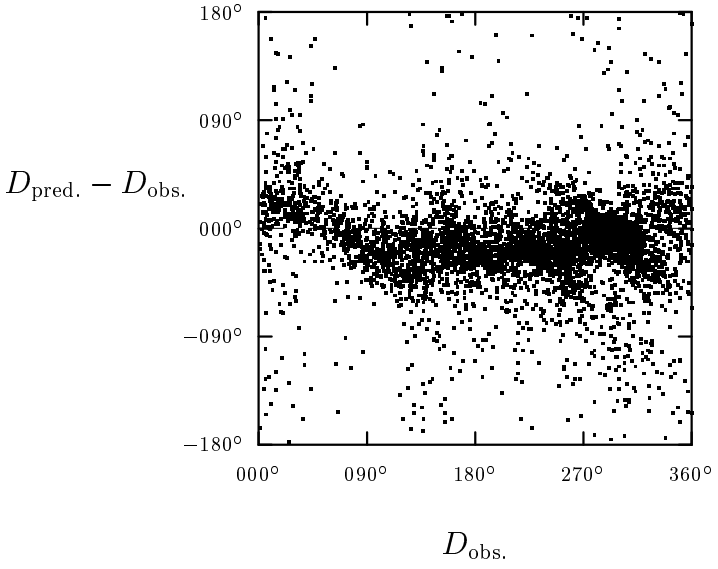

Figure 23. The difference between the predicted and the observed direction of the geostrophic wind, based on data from Børglum with A and B derived from the Tystofte-KEGERI data, and data from center number 8 (BOULBA).

predicted and observer geostrophic wind.

1. The derivation of the geostrophic drag law is based on the assumption that we have steady-state wind situation where the temporal derivatives in the equation of motion can be neglected. This assumption is certainly not always fulfilled.

2. It is also assumed that the geostrophic wind is constant with height, i.e. that we have a barotropic stratification. However, there are many situations where this is not the case and the implication then is that $\boldsymbol{G}$ does not in

an unambiguous way represents the *driving wind* aloft to be related to the surface wind.

3. The isobars may have strong curvature. This means that the geostrophic wind calculation from three pressure stations does not represent the real geostrophic wind inside the triangle, defined by the three stations. Consequently, it will be difficult to determine to which point in the triangle the calculated geostrophic wind actually pertains. This problem is particularly pronounced when to comparing surface winds at a station which is close to the edge of the triangle.

4. A strong curvature of the isobars may also introduce a centrifugal force in a balance with the pressure force and the Coriolis force. As we saw in section 5 this three-force balance implies that the wind aloft is better represented by the gradient wind than by the geostrophic wind. This means that in the drag law in these cases should be based on the surface wind and the gradient wind.

5. The temperature stratification in the atmospheric surface layer has a strong influence on the parameters A and B. According to the discussion and review by Jensen et al. (1984) the variation of these parameters as functions of $u_*/f/L$, where L is the Monin-Obukhov length, is particularly strong near neutral stratification ($|L| \to \infty$).

8 Concluding Remarks

It has been the purpose of this report to describe an installation of six pressure stations in Denmark and to point out how the records of ten-minute averages from these six stations can be exploited to study the climatology of the free wind and how it might vary geographically in Denmark.

The barometers are accurate and long-term stable within 0.1 HPa which at the Earth's surface corresponds to the weight per unit area of a column of air with a height of less than one meter. The positions and heights of the instruments have consequently been determined with a matching accuracy. We have even applied geometric equations pertaining to the local ellipsoid with the datum ED50 but, comparing to calculations using ordinary spherical geometry, this refinement seems of very little importance as long as the temperature correction of the pressure to a common reference height is carefully carried out. A test showed that distances of about 150 km can be off by 300 m. However, in this test the largest error was 0.9 m/s in a situation where the geostrophic wind speed was about 35 m/s and the direction error never exceeded 0.1°.

All six pressure stations were in operation on April 29 1998 and the recording continues. There has been some major interruptions at Balle and at Ulborg (see Fig. 1), mostly due to power failure and the present preliminary data analysis does not include data after March 23, 1999.

Using the equations from section 3 we have studied the geostrophic wind using ten triangles with centers distributed over a large part of Denmark (Fig. 7). (Six pressure-station positions can actually be corners in 20 different triangles, but many of them are rather flat.)

For each triangle we have calculated the mean of the geostrophic wind speed, irrespective of direction, and also in 12 direction sectors. Further, the Weibull

parameters have been determined sectorwise and for all directions. Apparently the means are in general larger the further we go west and it also seems that the largest means are found in the 300° sector.

We have also selected all the situations where at least one of the centers has its largest value of the geostrophic wind. There were three such situations, two where the largest values were in Jutland (Figs. 9 and 11) and one where it was just south of Zealand (Fig. 10). The first two indicate that the directions of the large geostrophic wind speeds were from SW to NW and that the magnitude of the speeds decrease with increasing longitude. The third case seems more inconclusive with small geostrophic wind speeds in Jutland and with no geographical uniformity in the directions.

If we want to take into account the curvature of the isobars we must include more than three pressure stations. As discussed in section 5, the six stations are just sufficient to determine the six coefficients if we assume that the surface pressure is a second order polynomial in the horizontal coordinates. The data have been analyzed from this point of view and the geostrophic wind speed, calculated from six pressure records G_6, has been compared to the geostrophic wind speed G_3 based on the pressure records at the three stations Kegnæs, Gedser, and Risø. There is a general agreement between G_6 and G_3 and between the directions as well. Also the gradient $\mathcal{G}$ wind has been determined from the six pressure records. We find, as expected, that most of the time $\mathcal{G}$ deviates from G_6 and G_3 more that these deviate from one another. This of course is no real surprise, but it may be important for future analyses since it could be more reasonable to use $\mathcal{G}$ rather than G as the external forcing of the surface wind.

The surface data at Tystofte has been used together with the pressure measurements at Kegnæs, Gedser, and Risø for reviewing the dimensionless constants A and B in the geostrophic drag law. We found that when the friction velocity is greater than 0.6 m/s, corresponding to a wind speed greater than about 8 m/s at the height 10 m over a uniform terrain with the roughness length 5 cm, then $A = 0.5$ and $B = 3.5$ are in good agreement with data. This should be compared to the values $A = 1.8$ and $B = 4.5$ used routinely for neutral stratification in WAsP. Taking this discrepancy as a measure of uncertainty, (100) and (102) imply that the uncertainties in predictions of the ageostrophic angle α and the geostrophic wind speed are about 5° and 10%, respectively.

With the values $A = 0.5$ and $B = 3.5$ we predicted the geostrophic wind from the Tystofte data and from the Børglum data. The first prediction is much better than the second, primarily for two reasons: the values of A and B were found on basis of the data we are using for the prediction in the Tystofte case, and Børglum is at the corner of the very triangle we use to determine the geostrophic wind.

Ultimately, we want to carry out an extreme-wind analysis on the geostrophic wind and the geographical variation of the 50-year event, similar to the analysis by Kristensen et al. (1999). However, the records we have so far are too short in duration to make such an analysis meaningful. From that point of view, we hope that the measurements will continue for at least 10 years.

We suggest that more pressure stations are put into operation. If we added pressure stations at say Helgoland in the North Sea, on the west side of Oslo Fjord, at Bornholm south of Sweden in the Baltic Sea, we would eventually be able to determine the geostrophic wind climate all the way to the borders of Denmark as can be seen by inspecting Figs. 1 and 7. Even with the records we have now and in the near future we find that the quality of the data is so good that it might be rewarding to let it form the basis of a Ph.D. study.

Acknowledgements

This project was funded by the EFP-project ENS–1363/97–004. Our colleagues Peter Kirkegaard, Jakob Mann, and Ole Rathmann have been helpful reviewing the equations. The last also provided the WAsP terrain description at Tystofte and Børglum. Arent Hansen has constructed the very efficient pressure stations and is to a large extent responsible for their smooth operation.

References

Dutton, J. A. (1986), *The Ceaseless Wind: An Introduction to the Theory of Atmospheric Motion*, Dover Publications, Inc, Mineola, NY 11501.

Jensen, N. O., Petersen, E. L. & Troen, I. (1984), Extraplolation of mean wind statistics with special regard to wind energy applications, Technical Report WCP-86, WMO/TD-15, World Meteorological Organization.

Kristensen, L., Rathmann, O. & Hansen, S. O. (1999), Extreme winds in Denmark, Technical Report R-1068(EN), Risø National Laboratory.

Mortensen, N. G., Landberg, L., Troen, I. & Petersen, E. L. (1993), Wind analysis and application program WA^{S}P, Technical Report I-666(EN), Risø National Laboratory. Vol 2: User's Guide.

Panofsky, H. A. & Dutton, J. A. (1984), *Atmospheric Turbulence: Models and Methods for Engineering Applications*, John Wiley & Sons, Inc., New York.

Rasmussen, L. M. (1996), Introduction til grafiske informationssystemer (introduction to geographical information systems), Technical Report FOFT F-9/1996, Danish Defence Research Establishment. In Danish.

Tennekes, H. (1982), Similarity relations, scaling laws and spectral dynamics, *in* F. T. M. Nieuwstadt & H. van Dop, eds, 'Atmospheric Turbulence and Air Pollution Modelling', D. Reidel Publishing Company, Dordrecht, Holland, Boston, U.S.A., London, England, chapter 2, pp. 37–68.

Tennekes, H. & Lumley, J. L. (1978), *A First Course in Turbulence*, The MIT Press, Cambridge, Massachusetts, and London, England. Fifth printing.

A Weibull Parameters

Here we present the means $\langle G \rangle$ and the Weibull parameters k and $\mathcal{A}$ for each 30° sector and all directions at the ten centers.

Table 8. Center 0, BOULKE.

D_G	$\langle G \rangle$	k	$\mathcal{A}$
000°	8.612	2.09892	9.723
030°	7.840	1.91368	8.837
060°	9.338	2.02168	10.539
090°	8.764	1.99902	9.889
120°	8.171	2.30483	9.223
150°	10.674	2.09030	12.051
180°	12.593	1.71061	14.120
210°	13.096	1.85102	14.745
240°	12.602	2.42948	14.212
270°	12.275	2.20500	13.860
300°	14.925	2.05396	16.848
330°	12.766	1.89449	14.385
000° − 330°	11.927	1.86121	13.431

Table 9. Center 1, BOULBA.

D_G	$\langle G \rangle$	k	$\mathcal{A}$
000°	9.542	2.06859	10.772
030°	8.828	1.70226	9.895
060°	8.927	2.38966	10.071
090°	9.347	2.31867	10.550
120°	9.386	2.40622	10.587
150°	10.790	1.81328	12.138
180°	10.733	1.85102	12.084
210°	11.540	2.04759	13.026
240°	12.271	2.14986	13.856
270°	13.364	2.11791	15.089
300°	15.822	2.18010	17.866
330°	11.536	1.81138	12.976
000° − 330°	12.003	1.90086	13.527

Table 10. Center 2, ULKEBA.

D_G	$\langle G \rangle$	k	$\mathcal{A}$
000°	8.672	1.65015	9.698
030°	8.164	1.77697	9.174
060°	7.920	1.75472	8.894
090°	9.919	2.02088	11.194
120°	8.290	2.10699	9.360
150°	9.857	1.99712	11.122
180°	10.797	1.81626	12.146
210°	12.060	1.83119	13.572
240°	13.147	2.19087	14.845
270°	12.511	2.25222	14.125
300°	14.117	2.15517	15.940
330°	11.671	1.93684	13.160
000° − 330°	11.548	1.89547	13.013

Table 11. Center 3, BOULRI.

D_G	$\langle G \rangle$	k	$\mathcal{A}$
000°	9.642	1.96840	10.876
030°	8.494	1.95439	9.580
060°	8.569	2.44884	9.662
090°	8.966	2.40622	10.114
120°	9.184	2.43613	10.357
150°	10.469	1.97202	11.810
180°	10.081	1.75341	11.320
210°	11.120	2.05894	12.553
240°	12.457	2.23083	14.065
270°	13.569	2.00896	15.312
300°	15.051	2.08790	16.993
330°	10.412	1.58790	11.605
000° − 330°	11.713	1.87250	13.193

Table 12. Center 4, ULKERI.

D_G	$\langle G \rangle$	k	$\mathcal{A}$
000°	8.812	1.71892	9.883
030°	7.250	1.62761	8.099
060°	7.696	2.01239	8.685
090°	9.740	1.99473	10.990
120°	8.677	2.13406	9.798
150°	8.354	2.03762	9.429
180°	9.444	1.90736	10.644
210°	10.923	1.97100	12.322
240°	12.521	2.09464	14.137
270°	11.564	2.28503	13.054
300°	12.348	2.15895	13.943
330°	10.727	1.80607	12.064
000° − 330°	10.590	1.92241	11.938

Table 13. Center 5, BOKEBA.

D_G	$\langle G \rangle$	k	$\mathcal{A}$
000°	13.301	1.76877	14.943
030°	9.706	1.93226	10.943
060°	7.633	2.02668	8.615
090°	9.995	2.62770	11.249
120°	10.483	2.28640	11.834
150°	10.107	2.20024	11.412
180°	9.943	2.03015	11.222
210°	11.043	1.98079	12.458
240°	12.634	2.33011	14.259
270°	13.502	2.31596	15.239
300°	14.175	2.14862	16.006
330°	13.771	2.02601	15.542
000° − 330°	12.071	2.02597	13.624

Table 14. Center 6, BAKEGE.

D_G	$\langle G \rangle$	k	$\mathcal{A}$
000°	9.217	1.72074	10.338
030°	7.416	1.58675	8.265
060°	7.323	1.81790	8.239
090°	9.457	2.21222	10.678
120°	9.960	2.18646	11.246
150°	9.423	2.03066	10.635
180°	9.398	1.77880	10.562
210°	9.838	1.73229	11.040
240°	12.881	2.20339	14.544
270°	13.389	2.12856	15.118
300°	13.403	2.20973	15.134
330°	9.842	1.84431	11.079
000° − 330°	11.226	1.90040	12.651

Table 15. Center 7, BAKERI.

D_G	$\langle G \rangle$	k	$\mathcal{A}$
000°	10.679	2.00032	12.050
030°	8.156	1.76948	9.163
060°	7.524	1.85800	8.472
090°	10.014	2.38631	11.297
120°	10.339	2.39729	11.663
150°	8.754	2.10051	9.884
180°	9.221	1.81451	10.373
210°	10.915	1.83554	12.285
240°	14.322	2.06863	16.168
270°	13.355	2.04820	15.075
300°	13.204	2.26820	14.906
330°	11.055	1.81497	12.436
000° − 330°	11.681	1.90779	13.165

Table 16. Center 8, KEGERI.

D_G	$\langle G \rangle$	k	$\mathcal{A}$
000°	8.811	1.60263	9.829
030°	6.969	1.52106	7.732
060°	7.807	1.59963	8.707
090°	9.177	2.05832	10.360
120°	9.464	2.33331	10.681
150°	9.030	2.16199	10.196
180°	8.967	1.85086	10.096
210°	9.730	1.77587	10.934
240°	11.551	2.15739	13.043
270°	12.521	2.15971	14.138
300°	12.947	2.00338	14.610
330°	9.941	1.84777	11.192
000° − 330°	10.556	1.88320	11.892

Table 17. Center 9, BAGERI.

D_G	$\langle G \rangle$	k	$\mathcal{A}$
000°	10.832	1.77912	12.173
030°	8.564	1.99011	9.663
060°	7.747	1.99874	8.741
090°	9.725	2.52800	10.958
120°	10.395	2.39181	11.727
150°	9.662	2.11314	10.909
180°	9.592	1.81236	10.790
210°	13.472	1.94513	15.192
240°	13.107	2.02231	14.792
270°	12.409	2.24255	14.010
300°	13.189	2.08694	14.890
330°	12.824	1.72751	14.388
000° − 330°	11.726	1.92551	13.220

Bibliographic Data Sheet **Risø–R–1145(EN)**

Title and author(s)

Geostrophic Winds in Denmark: a preliminary study

Leif Kristensen and Gunnar Jensen

ISBN	ISSN
87–550–2616–8	0106–2840

Dept. or group	Date
Department of Wind Energy and Atmospheric Physics	November 22, 1999

Groups own reg. number(s)	Project/contract No.
1105021–04	ENS–1363/97–0004

Pages	Tables	Illustrations	References
43	17	23	8

Abstract (Max. 2000 char.)

High-precision barometers have been deployed at six sites in Denmark, four west and two east of the Great Belt. The purpose is to establish long climatological records of the geostrophic wind as a supplement to the records of tens of years of duration of surface observations of wind, temperature, humidity etc., which have been obtained by Risø at many sites in Denmark. Three of these sites are in principle sufficient to determine an average of the magnitude and direction of the geostrophic wind inside the triangle formed by the three sites. Ten, out of twenty possible, triangles have been selected as suitable for studying the geographical variations of the geostrophic wind. A tentative conclusion from about one year of data is that statistically the geostrophic wind decrease in magnitude when going from west toward east. The data also showed that the largest mean values of the geostrophic mean wind speed are in a direction sector from 285° to 315°. The Weibull parameters were calculated for all ten triangles. The curvature of the isobars were determined by using simultaneous pressure measurements at all six sites and the geostrophic and gradient winds were calculated and compared to the geostrophic wind based on three pressure measurements in one particular triangle. Combining the geostrophic wind with the surface wind measured at Tystofte in southern Zealand, the two dimensionless constants A and B in the geostrophic drag law were determined as functions of the surface friction velocity. These data suggest that $A = 0.5$ and $B = 3.5$. The surface data at Tystofte and at Børglum in Vendsyssel in northern Jutland were used to predict the geostrophic wind by applying the geostrophic drag law with these constants and the predictions were compared to the observed geostrophic wind.

Descriptors INIS/EDB

ATMOSPHERIC PRESSURE; BAROMETERS; DENMARK; DRAG; GEODESY; VELOCITY; WIND

Available on request from Information Service Department, Risø National Laboratory (Afdelingen for Informationsservice, Forskningscenter Risø), P.O. Box 49, DK–4000 Roskilde, Denmark.
Phone +45 46 77 40 04, Fax +45 46 77 40 13, E-mail infserv@risoe.dk